Disconnecting prefrontal cortical neurons from the ventral midline thalamus: Loss of specificity due to progressive neural toxicity of an AAV-Cre in the rat thalamus

Élodie Panzer, Laurine Boch, Brigitte Cosquer, Iris Grgurina, Anne-Laurence Boutillier, Anne Pereira de Vasconcelos, Aline Stephan, Jean-Christophe Cassel

Journal of Neuroscience Methods 405 (2024) 110080

Contents lists available at ScienceDirect

Journal of Neuroscience Methods

journal homepage: www.elsevier.com/locate/jneumeth

Disconnecting prefrontal cortical neurons from the ventral midline thalamus: Loss of specificity due to progressive neural toxicity of an AAV-Cre in the rat thalamus

Elodie Panzer [a,b], Laurine Boch [a,b], Brigitte Cosquer [a,b], Iris Grgurina [a,b], Anne-Laurence Boutillier [a,b], Anne Pereira de Vasconcelos [a,b,1], Aline Stephan [a,b,*,1], Jean-Christophe Cassel [a,b,*,1]

[a] Laboratoire de Neurosciences Cognitives et Adaptatives, Université de Strasbourg, Strasbourg F-67000, France
[b] LNCA, UMR 7364 - CNRS, Strasbourg F-67000, France

ARTICLE INFO

Keywords:
Adeno-associated virus – Caspase – Cre recombinase – Disconnection – Thalamus – Toxicity

ABSTRACT

Background: The thalamic reuniens (Re) and rhomboid (Rh) nuclei are bidirectionally connected with the medial prefrontal cortex (mPFC) and the hippocampus (Hip). Fiber-sparing N-methyl-D-aspartate lesions of the ReRh disrupt cognitive functions, including persistence of certain memories. Because such lesions irremediably damage neurons interconnecting the ReRh with the mPFC and the Hip, it is impossible to know if one or both pathways contribute to memory persistence. Addressing such an issue requires selective, pathway-restricted and direction-specific disconnections.

New method: A recent method associates a retrograde adeno-associated virus (AAV) expressing Cre recombinase with an anterograde AAV expressing a Cre-dependent caspase, making such disconnection feasible by caspase-triggered apoptosis when both constructs meet intracellularly. We injected an AAVrg-Cre-GFP into the ReRh and an AAV5-taCasp into the mPFC. As expected, part of mPFC neurons died, but massive neurotoxicity of the AAVrg-Cre-GFP was found in ReRh, contrasting with normal density of DAPI staining. Other stainings demonstrated increasing density of reactive astrocytes and microglia in the neurodegeneration site.

Comparison with existing methods: Reducing the viral titer (by a 4-fold dilution) and injection volume (to half) attenuated toxicity substantially, still with evidence for partial disconnection between mPFC and ReRh.

Conclusions: There is an imperative need to verify potential collateral damage inherent in this type of approach, which is likely to distort interpretation of experimental data. Therefore, controls allowing to distinguish collateral phenotypic effects from those linked to the desired disconnection is essential. It is also crucial to know for how long neurons expressing the Cre-GFP protein remain operational post-infection.

1. Introduction

Historically, the about 60 nuclei forming the thalamus have been distinguished according to whether their projections concentrate on restricted cortical regions or are diffuse (Lorente de No, 1938). The former were attributed to a *specific* subdivision of the thalamus, the latter to a *non-specific* one, a view that has nevertheless been challenged since then (Bentivoglio et al., 1991; Groenewegen and Berendse, 1994). The reuniens (Re) and rhomboid (Rh) nuclei are part of the non-specific thalamus; they belong to its ventral midline roofing the third ventricle. The Re projects to – and receives afferents from – more than 50 different brain regions. The Rh also projects to about 50 brain regions, but the regions providing its innervation are more limited in number (e.g., Cassel et al., 2021). Within this rich connectivity network, the ReRh nuclei occupy an ideal position in the bidirectional information flow between the medial prefrontal cortex (mPFC) and the hippocampus (Hip). The Hip provides monosynaptic input to the mPFC (Hoover and Vertes, 2007; Jay and Witter, 1991), which is not the case the other way around (e.g., Vertes, 2004). From mPFC to Hip, signals cross more than one synapse, with a relay in e.g., the entorhinal cortex or the ReRh

* Correspondence to: LNCA – UMR 7364, Faculté de Psychologie, 12 rue Goethe, Strasbourg F-67000, France.
E-mail addresses: aline.stephan@unistra.fr (A. Stephan), jcassel@unistra.fr (J.-C. Cassel).
[1] With equivalent contribution

https://doi.org/10.1016/j.jneumeth.2024.110080
Received 28 September 2023; Received in revised form 17 January 2024; Accepted 14 February 2024
Available online 16 February 2024

nuclei (e.g., Xu and Südhof, 2013).

If one is focusing in more detail on this connectivity network, it is to note that the ReRh nuclei have bidirectional connections with both the Hip (more with its ventral than dorsal region and only with CA1 neurons) and the mPFC (i.e., anterior cingulate, infralimbic, prelimbic regions). Furthermore, a small proportion (5–10%) of Re neurons send collaterals to both structures (Hoover and Vertes, 2012; Varela et al., 2014). Electrophysiological data demonstrate that the Re produces hippocampo-cortical synchronization of beta, delta, gamma and theta oscillations during a variety of cognitive tasks (Dolleman-van Der Weel et al., 2019; Jayachandran et al., 2023). More than a decade ago, we found (Loureiro et al., 2012), and later confirmed (Ali et al., 2017; Klein et al., 2019; Quet et al., 2020), that N-methyl-D-aspartate lesions of the ReRh nuclei disrupted remote memory for spatial and contextual information without altering encoding or persistence of recent memory. These findings demonstrate a contribution of the ReRh to systems-level consolidation and endurance of some types of memory (e.g., Cassel et al., 2013; Ferraris et al., 2021).

In our previous work (Ali et al., 2017; Klein et al., 2019; Loureiro et al., 2012; Quet et al., 2020), we performed N-methyl-D-aspartate lesions and the damage therefore disrupted projections from the ReRh to both the mPFC and Hip indistinctly and, at the same time, removed potentially important targets for projections arising therefrom. Therefore, it was impossible to know if one of these connecting pathways (e.g., from mPFC to ReRh) is more involved in systems-level consolidation than another (e.g., from ReRh to Hip or ReRh to mPFC) or, as an alternative, if the whole system operates in a closed loop to support memory persistence. To address such an issue, it would be necessary to perform selective, pathway-restricted and direction-specific disconnections. By associating a retrograde adeno-associated virus (AAV) expressing Cre recombinase with an anterograde AAV expressing a Cre-dependent caspase (Yang et al., 2013), such disconnection becomes possible, as shown previously in other brain systems (e.g., Basting et al., 2018; Laurent et al., 2017; Marciante et al., 2020; Nadel et al., 2020; Walker et al., 2022).

In the current study, we started surgeries by using the virus preparations at half the concentration recommended by the supplier (i.e., 2.5×10^{13} GC/mL). AAVrg-Cre-GFP was injected into ReRh nuclei, AAV5-taCasp into medial mPFC. We were able to establish that, at the concentrations used, AAVrg-Cre-GFP caused protracted but ultimately severe neurodegeneration in and around the injection site. In addition, a DAPI staining failed to highlight this lesion because of an important glial infiltration in the area of neuronal loss, glial nuclei compensating for the lost neuronal ones. The lesion area was clearly evidenced with an immunostaining of the nuclear neuronal protein NeuN. To the best of our knowledge, this is the first study to provide evidence for AAVrg-Cre-GFP toxicity in the ReRh nuclei. Recent work had shown similar consequences after injections of AAVrg-Cre-GFP in the ventral tegmental area (Erben et al., 2022) or the substantia nigra (Rezai Amin et al., 2019), what, with our results, suggests a possibly region-independent neuronal toxicity of the viral construct.

In the following experiments we aimed to elucidate the dynamic of this neurotoxicity by analyzing the impact of AAVrg-Cre-GFP at different post mortem delays; 1 week, 2.5 weeks, 5 and 10 weeks. We quantified various parameters such as viral infection area, neuronal loss expanse, and glial response. After all, we managed to find appropriate viral infection parameters that would permit selective damage to prefrontal neurons projecting to the ReRh.

2. Experimental procedures

The study encompassed 4 experiments. In the first one, the AAVrg-Cre-GFP was injected into the ReRh at half the titration provided by the supplier. In the second experiment, the effects of the AAVrg-Cre-GFP were followed over 10 weeks, with verifications at 1, 2.5, 5 and 10 weeks post-injection. In the third experiment, we tested different titrations at a single post-infection delay (i.e., 5 weeks). In the fourth experiment, we verified that the combination of the AAV5-taCasp and the AAVrg-Cre-GFP at a possibly non-toxic titration for the ReRh leads to damage affecting the cortico-thalamic pathway.

2.1. Animals

All experimental animals were used in compliance with the rules of the European Community Council Directive (2010/63/EU) and the French Agriculture Ministry. All approaches have been validated by the ethical committee of the University of Strasbourg (CREMEAS—authorizations #13261–2018012918394046). We used 45 adult Long–Evans male rats (Janvier Labs, Le Genest-Saint-Isle, France) weighing between 130 and 250 g at their arrival at the laboratory (they were 4–7 weeks old). The rats were housed 2 or 3 per cage in quiet facilities, under a 12-h light/dark cycle (light on at 7:00 a.m.) with food and water ad libitum, controlled temperature (22°C), and a hygrometry of about 55%. Before any experimental manipulation, rats were individually handled for 2 min/day over five consecutive days. We used 9 rats for the first experiment (Exp 1: 6 for the mPFC injection and 3 for the ReRh injection); 16 rats for the time-course experiment (Exp 2: 1 week, n = 6; 2.5 weeks, n = 6; 10 weeks, n = 4), 20 rats for testing different titrations (Exp 3: initial titer divided by 4, 8, 20 and 200; T/4, n = 4; T/8, n = 4; T/20, n = 6; T/200, n = 6, respectively). Experiment 4 focused on histological material from the 4 rats of the T/8 group of experiment 3.

2.2. Virus

The viral vector carrying the floxed caspase gene was the anterograde AAV5. EF1a.Flex-taCasP3-TEVp (UNC Gene Therapy Center-Vector Core), AAV5-taCasp hereafter. It was diluted twice in PBS from the stock solution (4.2×10^{12} particles/mL). The viral vector carrying the Cre-recombinase gene was the retrograde AAVrg.hSyn.eGFP-Cre-WPRE-SV40 (Addgene, MA, USA), AAVrg-Cre-GFP hereafter. For Exp 1, it was diluted twice in PBS from the stock solution (2.5×10^{13}), despite Addgene's recommendation to use the stock solution as is for in vivo experiments. For precise dilution see Table 1. This retrograde serotype has been engineered by Tervo et al. (2016) from an AAV2.

2.3. Sodium dodecyl sulfate-polyacrylamide gel electrophoresis (SDS-PAGE)

This electrophoresis has been done in order to verify the purity of our AAVrg-Cre-GFP sample.

5 μL of AAVrg-Cre-GFP virus (AAVrg.hSyn.eGFP-Cre-WPRE-SV40, Addgene, MA, USA) was mixed with 4X Laemmli buffer (Bio-rad, #1610747), with addition of 1/10 β-mercaptoethanol (Sigma-Aldrich, #444203), to obtain a final 1X solution that was heated at 100°C for 4 min. Virus was then loaded on Midi-PROTEAN TGX Stain-Free™ Precast Gel (26 wells, 4–20%, Bio-Rad #5678095) and left to migrate for 40 min, at 150 V. This was followed by a UV-induced 1-min activation of the gel, using a ChemiDoc molecular imager (Bio-Rad), producing fluorescence that allows for visualization of the viral proteins on the gel.

2.4. Stereotactic Injections

After one week of acclimatization and another week of daily manipulation of the rats, the viral vectors were stereotactically injected in the brain. When unilateral, as in the mPFC, there was no injection on the contralateral side; for the illustrations shown in Supplementary Figure 6, rats received bilateral injections of the AAV-Cre in the mPFC (2 sites/side, 0.5μL/site for a post-surgical delay of 5 weeks; 3 sites/side, 0.6 μL/site for a post-surgical delay of 10 weeks). For all surgeries, rats were anesthetized with Isoflurane (Isoflu-Vet®, Dechra, 4% for induction and 1.5% for maintenance) and placed into the stereotactic frame. Viral injections targeting the ReRh or the mPFC were made using slow

Table 1
Summary table of viruses used, their characteristics, rhe initial titer, the injected titers, the injected volumes and the corresponding illustrations. Abbreviations: Hip = hippocampus; mPFC = medial prefrontal cortex; Suppl = supplementary; T = titer; wks = weeks (concerns duration of post-injection survival time). Note that for the 10-week delay in our second experiment, the AAV-Casp has been injected into the dorsal hippocampus (Hip).

Experiment	Associated figure (s)	Delay	Virus	Serotype	Promoter	Reference (website)	Plasmid	Structure	Used titer (vg/mL)	Injected volume	Coordinates
1	1, 2, 4, 5, 6	5 wks	AAV-taCasp	5	EF1α	https://www.me d.unc.edu/genet herapy/vectorco re/in-stock-aavvectors/shah/	pAAV.EF1a.flex-taCasp3-TEVp. WPRE.hGH	mPFC	2.1×10^{12}	2×0.5μL (unilateral)	AP: +3.00 mL: +0.5 DV: −4.6 and −3.6
			AAV-Cre-GFP	retrograde	hSyn	https://www.addgene.org/105540/	pENN.AAV.hSyn. HI.eGFP-Cre.WPRE. SV40	ReRh	1.25×10^{13}	2×1μL	AP: −1.8 and −2.3 mL: −1.9 DV: −7.1 and −7.2 Angle of 15°
2	3, 4, 5, 6	1 and 2.5wks	AAV-taCasp	5	EF1α	https://www.me d.unc.edu/genet herapy/vectorco re/in-stock-aavvectors/shah/	pAAV.EF1a.flex-taCasp3-TEVp. WPRE.hGH	mPFC	2.1×10^{12}	3×0.6μL (unilateral)	AP: +3.00 mL: +0.5 DV: −5, −3.8 and −2.2
			AAV-Cre-GFP	retrograde	hSyn	https://www.addgene.org/105540/	pENN.AAV.hSyn. HI.eGFP-Cre.WPRE. SV40	ReRh	1.25×10^{13}	2×1μL	AP: −1.7 and −2.2 mL: −1.9 DV: −7.1 and −7.2 Angle of 15°
		10 wks	AAV-taCasp	5	EF1α	https://www.me d.unc.edu/genet herapy/vectorco re/in-stock-aavvectors/shah/	pAAV.EF1a.flex-taCasp3-TEVp. WPRE.hGH	Hip	2.1×10^{12}	2×1μL (unilateral)	AP: −5.4 mL: −3.5 DV: −9.2 and −3.2
			AAV-Cre-GFP	retrograde	hSyn	https://www.addgene.org/105540/	pENN.AAV.hSyn. HI.eGFP-Cre.WPRE. SV40	ReRh	1.25×10^{13}	2×1μL	AP: −1.7 and −2.2 mL: −1.9 DV: −7.1 and −7.2 Angle of 15°
3	7	5 wks	AAV-taCasp	5	EF1α	https://www.me d.unc.edu/genet herapy/vectorco re/in-stock-aavvectors/shah/	pAAV.EF1a.flex-taCasp3-TEVp. WPRE.hGH	mPFC	2.1×10^{12}	3×0.6μL (unilateral)	AP: +3.00 mL: +0.5 DV: −5, −3.8 and −2.2
			AAV-Cre-GFP	retrograde	hSyn	https://www.addgene.org/105540/	pENN.AAV.hSyn. HI.eGFP-Cre.WPRE. SV40	ReRh	From 1.25×10^{13} to 1.25×10^{11}	2×0.5μL	AP: −1.8 and −2.3 mL: −1.9 DV: −7.1 and −7.2 Angle of 15°
4	7, 8	5 wks	AAV-taCasp	5	EF1α	https://www.me d.unc.edu/genet herapy/vectorco re/in-stock-aavvectors/shah/	pAAV.EF1a.flex-taCasp3-TEVp. WPRE.hGH	mPFC	2.1×10^{12}	3×0.6μL (unilateral)	AP: +3.00 mL: +0.5 DV: −5, −3.8 and −2.2
			AAV-Cre-GFP	retrograde	hSyn	https://www.addgene.org/105540/	pENN.AAV.hSyn. HI.eGFP-Cre.WPRE. SV40	ReRh	3.125×10^{12}	2×0.5μL	AP: −1.8 and −2.3 mL: −1.9 DV: −7.1 and −7.2 Angle of 15°

(*continued on next page*)

Table 1 (*continued*)

Experiment	Associated figure (s)	Delay	Virus	Serotype	Promoter	Reference (website)	Plasmid	Structure	Used titer (vg/mL)	Injected volume	Coordinates
//: thalamo-cortical disconnection	Suppl Fig. 6	5 wks	AAV-taCasp	5	EF1α	https://www.me d.unc.edu/genetherapy/vectorco re/in-stock-aavvectors/shah/	pAAV.EF1a.flex-taCasp3-TEVp.WPRE.hGH	PeriRe	2.1×10^{12}	1×1μL	AP: −2.6 mL: +0.6 DV: −7.6
			AAV-Cre-GFP	retrograde	hSyn	https://www.addgene.org/105540/	pENN.AAV.hSyn.HI.eGFP-Cre.WPRE.SV40	mPFC	1.25×10^{13}	2×0.5μL (in each hemisphere)	AP: +3.00 mL: +/- 0.5 DV: −4.6 and −3.6
		10 wks	AAV-taCasp	5	EF1α	https://www.me d.unc.edu/genetherapy/vectorco re/in-stock-aavvectors/shah/	pAAV.EF1a.flex-taCasp3-TEVp.WPRE.hGH	PeriRe	2.1×10^{12}	1×1μL	AP: −2.6 mL: +0.6 DV: −7.6
			AAV-Cre-GFP	retrograde	hSyn	https://www.addgene.org/105540/	pENN.AAV.hSyn.HI.eGFP-Cre.WPRE.SV40	mPFC	1.25×10^{13}	3×0.6μL (in every hemisphere)	AP: +3.00 mL: +/- 0.5 DV: −5, −3.8 and −2.2

microinfusions (over 5 min) via a silicium infusion needle (30 G, Phymep). When both the mPFC and the ReRh were to be injected in the same animal, the surgeries were done in a single session. After leaving the needle in situ for an additional 5 min to ensure diffusion of the virus in the target structure, it was slowly retracted. Infusion sites were at the following coordinates (in mm): AP - 1.8 and- 2.3 (from bregma), DV −7.1 and −7.2 (from skull), mL 1.9 (from midline of the sagittal sinus) for the ReRh, and for the mPFC, AP 3.0, DV −5.0, −3.8 and −2.2, and mL 0.5 and −0.5 (Paxinos and Watson, 2017) for all delays but 5 weeks; for the postsurgical delay of 5 weeks, only 2 injections were made on each side at DV −4.6 and −3.6 mm. In Exp 3, the vertical coordinates for the mPFC injections corresponded to those with the 3 sites/side. Finally, for ReRh sites, as the nuclei are medial, we used an angle of 15° to avoid damaging the venous sinus. More detail is given in Table 1 (volume, exact coordinates, etc).

After the last infusion, the scalp was sutured. All rats that underwent surgery were allowed to recover under a warm lamp for –30 min before being placed back into their homecage.

2.5. Histology

2.5.1. Perfusion and tissue sectioning

All rats were subjected to a lethal dose of ketamine (200 mg/kg, i.p.) and xylazine (30 mg/kg, i.p.) and perfused transcardially with a cold (4°C) 4% paraformaldehyde (PFA) solution. Brains were removed and transferred to a 20% sucrose solution for 48 h at 4°C before being snap frozen (in isopentane, −40°C) and subsequently stored at −80°C. Serial coronal sections (40μm) were cut through the prefrontal cortex and the midline thalamus using a cryostat at −20° C (Leica CM3050S). The sections were kept floating in a cryoprotective solution at −80°C until being processed for histological staining.

2.5.2. Fluorescent Immunohistochemistry

The localization and extent of the viral infection could be observed directly under a fluorescence microscope, without any immunostaining. However, a NeuN protein immunostaining was performed in order to facilitate the observation of the different brain regions. Some sections were also immunostained for calretinin and calbindin, two neuronal cytoplasmic proteins. Sections were also stained for either GFAP (a marker of astrocytes) or Iba1 (a marker for microglia). Anti-GFP immunostaining was performed in the mPFC.

Every immunostaining was performed on free-floating brain sections evenly distributed along the entire rostro-caudal extent of the ReRh or the mPFC, as previously described (e.g. Klein et al., 2019). Briefly, sections were rinsed three times during 10 min in a PBS merthiolate buffer before being soaked for 1 h in 5% normal horse serum in PBS containing 0.5% Triton X-100. The sections were then transferred into the primary antibody solution and kept overnight at room temperature. Then, they were rinsed 3×10 min in PBS, and soaked for 2 h in a buffer solution containing the secondary antibody. Finally, they were rinsed three times in PBS (the second rinsing contained DAPI to stain cell nuclei) and mounted with Mowiol® (Sigma Aldrich).

All the antibodies used are described in Table 2.

2.5.3. Image acquisition

All images were acquired with Axio Imager (Zeiss), an epifluorescent microscope equipped with a motorized x–y–z stage control. Mosaics were performed using the Zen (Zeiss) software. The same light intensity and exposure time were used for all sections. Focus was made on the NeuN channel, and parameters were determined according to the strongest signal. Areas of interest in stained sections were taken using a 10x objective.

2.5.4. Quantification

All quantifications were done with the free access software QuPath (e.g., Bankhead et al., 2017; Humphries et al., 2021). It is noteworthy

Table 2
Methodological precisions about the antibodies used for the various immunostainings performed in our four experiments.

Antibody against	Host species	Provided by	Catalog reference	Conjugated fluorochrome	Incubation dilution
GFAP	Rabbit	Millipore	AB5804	None	1/1000
Iba1	Guinea Pig	Synaptic systems	HS-234 004	None	1/500
NeuN	Mouse	Millipore	MAB377	None	1/1000
Calretinin	Mouse	Swant	6B3	None	1/1000
Calbindin	Rabbit	Millipore	ABN2192	None	1/500
Guinea Pig	Goat	Invitrogen	A21450	Alexa Fluor 647	1/500
Rabbit	Goat	Invitrogen	A32733	Alexa Fluor 647	1/500
Mouse	Donkey	Invitrogen	A32744	Alexa Fluor	1/1000

that we did not use an unbiased stereological method. Instead, quantification was performed with freely available software. As the immunostainings were not processed in a single batch, differences in fluorescence signal were normalized with visualization parameters. The quantifications were done on 7–12 slides (mean: 9.11) per rat for GFP and NeuN, on 3–9 slides (mean: 4.58) per rat for Iba1, and on 4–8 slides (mean: 4.78) per rat for GFAP. If not stated otherwise, we then calculated the mean of all slides for a single rat, before calculating the mean of all rats of every group.

2.5.5. Area delineation

In order to estimate the extent of the viral infection, neuronal loss, and glial responses, we outlined the associated regions with the "Polygon" tool (see Supplementary Fig. 1). To avoid any bias, we only selected the channel of interest (e.g.: Alexa Fluor 594 for neuronal loss) and outlined the region for every rat of every group (1WK, 2.5WKS, 5WKS, 10WKS) before starting the next channel.

2.5.6. Intensity measurements

The intensity of the GFP fluorescent signal was quantified with the "Add intensity features" tool of QuPath, in every viral infection area. The parameters were as follows: Preferred pixel size: 2 μm; Region: ROI; Tile diameter: 25 μm; Channels: GFP; Basic features: Mean; Haralick distance: 1; Haralick number of bins: 32.0.

2.5.7. Cell density

In order to evaluate the density of the different cell types (neurons, astrocytes, microglia), we used the "Classifier" tool. We first run the StarDist extension script, which was trained to detect and segment nuclei on a DAPI staining (Weigert et al., 2020).

Once the nuclei were detected, we trained a classifier to sort the nuclei that showed positive to another staining, for example the (DAPI+NeuN)-positive nuclei were sorted as neurons (see Supplementary Fig. 1). This training was made on 1 slide per rat, by one experimenter per channel, and in shades of grey to facilitate visualization of contrasts. For the reasons mentioned above, we trained a different classifier for every immunostaining batch. Once the classifier was trained, it was run on the viral infection area of every slide.

2.6. Statistical analyses

Unless otherwise specified and depending on the experiment, data analyses used Student's t tests or two-way ANOVAs, with repeated measures where appropriate. Likewise, where appropriate, these analyses were completed by multiple comparisons using the Newman–Keuls multiple range test. In the case of non parametric distributions, we used a Kruskal-Wallis (K-W) test, followed by a Dunn multiple comparisons test. Homogeneity of variance and normality of distribution were tested systematically. Values of $p < 0.05$ were considered significant.

3. Results

3.1. Experiment 1: Retrograde AAVrg-Cre-GFP injections into the ReRh nuclei combined with intracortical injections of anterograde AAV5-taCasp

We injected 2×1 μL of the retrograde AAVrg-Cre-GFP preparation into the ReRh nuclei. The injected solution had a titer of 1.25×10^{13} vg/mL. This is half the titer preconized by Addgene, although in the website catalog, the viral solution is proposed for use in living animals as provided. It is also noteworthy that studies published in the literature have used titers $> 10^{12}$ vg/mL, with injection volumes usually of the μL order (e.g., Cearley and Wolfe, 2007; Chen et al., 2021; Shen et al., 2016, Stewart et al., 2021; see also Erben et al., 2022 regarding the titer). All of our rats injected with the AAVrg-Cre-GFP also received a unilateral injection of the AAV5-taCasp (2×0.5 μL) into the medial prefrontal cortex (mPFC), using a solution with a titer of 2.1×10^{12} vg/mL. The contralateral side was left unoperated and served as control. The rats were kept for a post-surgical survival time of 5 weeks. Histological observations are illustrated in Figs. 1 and 2.

In the mPFC, we found a reduction of the number of GFP-positive cells on the side in which the AAV5-taCasp had been injected as compared to the contralateral hemisphere (Fig. 1). These GFP-positive cells were quantified, and the resulting data analyzed using a t-test for paired samples. On the side injected with the AAV5-taCasp, the number of GFP-positive neurons was reduced by about 40% in average as compared to the contralateral hemisphere. Statistical analyses considering the 21 sections from the 3 rats (7 per rat) with correct injections showed that this difference was significant ($t_{(20)} = 5.385$, $p < 0.001$; Fig. 1). It is noteworthy that, in contrast to the ReRh nuclei, where the virus also carries a reporter gene that reflected the localization and extent of infection, in the mPFC the extent of infection could only be visualized indirectly (i.e., by the reduction in the number of GFP-positive neurons). Indeed, the caspase gene is too large to associate a reporter gene with it in an AAV.

In the ventral midline thalamus (VMT), we induced a widespread transduction of the AAVrg-Cre-GFP, as illustrated by the localization of GFP-positive cells within and in the close vicinity of the ReRh nuclei (Fig. 2a, 2b). The brain sections through the VMT were processed for DAPI staining and anti-NeuN immunostaining. DAPI staining appeared normal in the region infected with the AAVrg-Cre-GFP (Fig. 2c, 2d). Indeed, the stained nuclei showed no abnormal density in comparison with surrounding regions. This infected region, however, was almost completely devoid of NeuN-positive cells (Fig. 2d, 2e, 2f), possibly indicating an unexpected loss of neurons in the region confined to the spread of the infection. Such loss would point to neuronal toxicity of the AAVrg-Cre-GFP construct in a region roughly corresponding to the viral infection. Supplementary Fig. 2 and 3 provide illustrations with larger magnifications of the same kind of material.

As we could not exclude that this toxicity might have been related to an alteration of the viral construct, we checked that the construct had not been altered. We used a sodium dodecyl sulfate–polyacrylamide gel electrophoresis (SDS-PAGE). It resulted in the separation of all the proteins into three distinct bands corresponding to the three AAV-capsid proteins VP1, VP2 and VP3 (see supplementary Fig. 4). The absence of

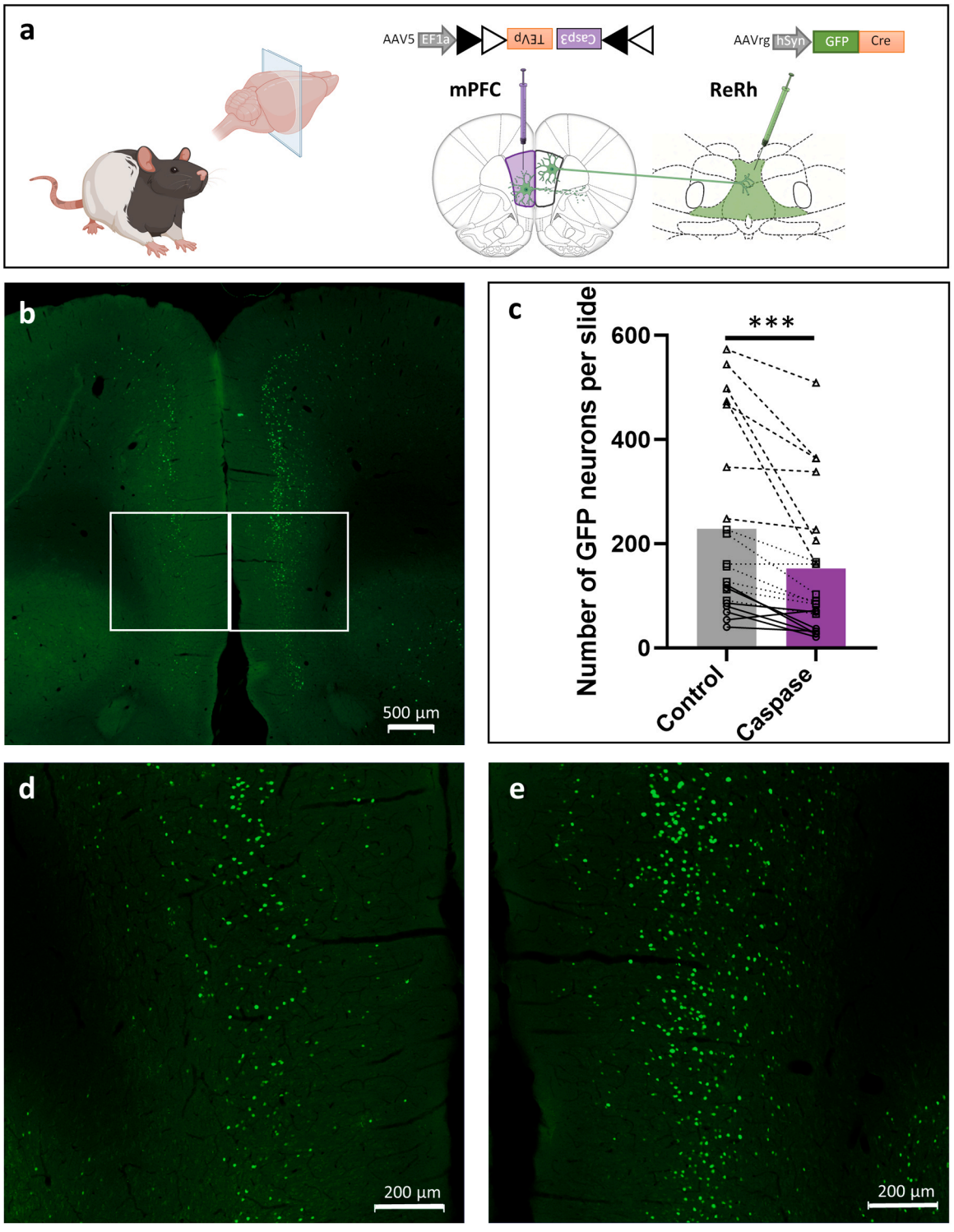

Fig. 1. **(a)** Surgical protocol used in Experiment 1. The AAV containing the floxed caspase gene was injected unilaterally into the medial prefrontal cortex (mPFC) of Long-Evans male rats, which also received an injection into the reuniens and rhomboid (ReRh) nuclei of the virus containing the Cre-GFP gene coding for the fluorescent fusion protein. **(b)** Image showing GFP-positive neuronal nuclei in the mPFC. **(d)** and **(e)** are higher magnifications of the cortical regions delimited by squares in (b); (d) is showing the side in which the AAV5-taCasp has been injected; the contralateral side (e) is used as the non-injected control. Scale bars are shown directly on the photographs. **(c)** Number of neurons counted in each section prepared from the brain of 3 rats; open circles joined by solid lines are from one rat, open triangles joined by dashed lines are from another rat, and open squares from the last rat are joined by stippled lines. The bars show the average value on the side injected with the AAV-taCasp (left) and its contralateral control (right). Statistical analysis: ***, $p < 0.001$. There is a relatively large inter-individual variability, which most probably reflects variability across infection degrees within the ReRh nuclei and thus across slices.

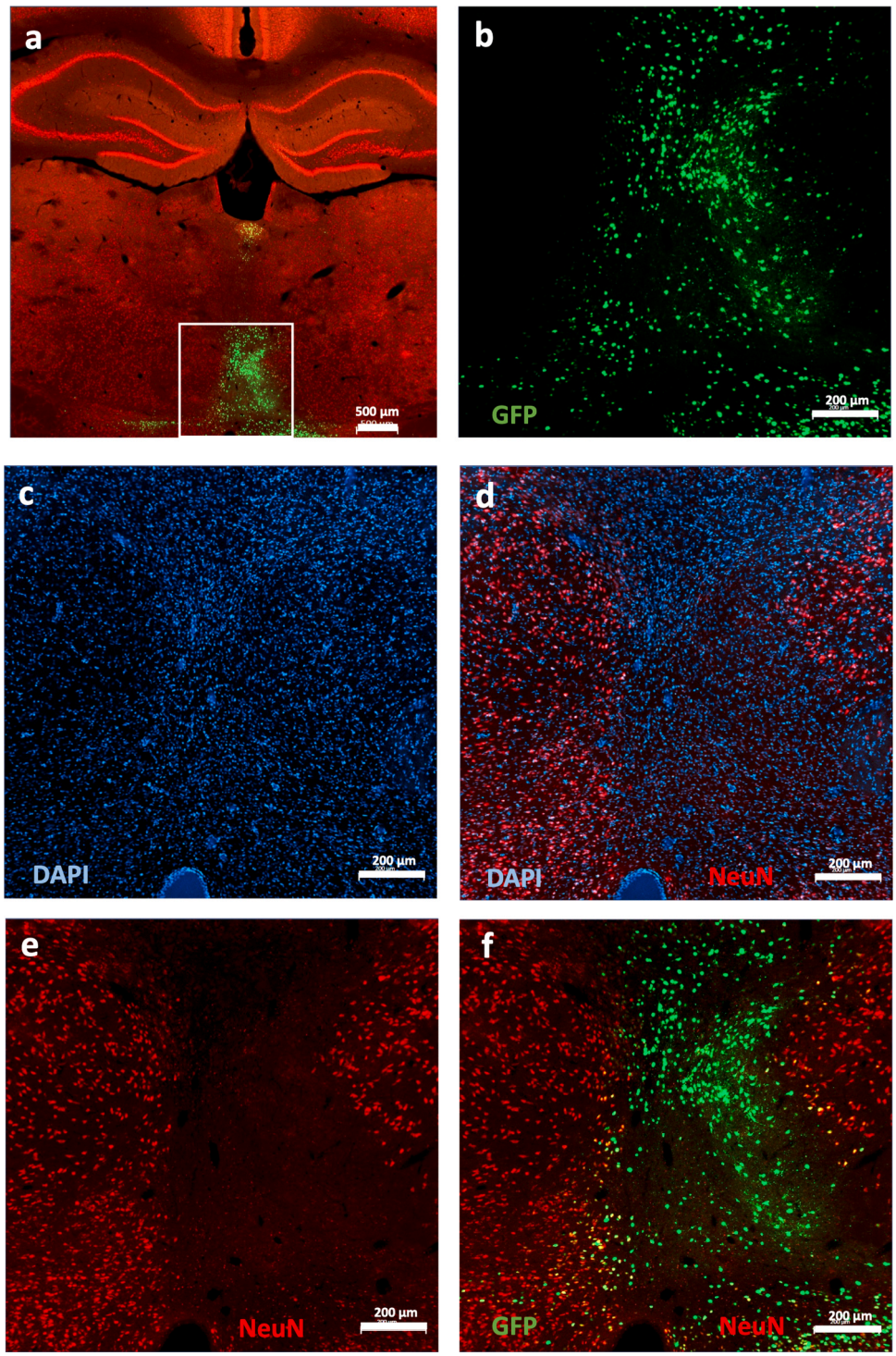

Fig. 2. **(a)** Images showing the localization of the transduction in the ReRh nuclei in a section immunostained for the neuronal nuclear protein NeuN. The post-surgical survival time was of 5 weeks; all photographs are from the same section. **(b)** is a higher magnification of the thalamic region delimited by the square in (a); only GFP staining is shown. **(c)** same region as in (b) with focus on DAPI staining in the ventral midline thalamus. **(d)** same region as in (b) and (c) with DAPI and NeuN staining merged; notice that there is a DAPI-positive region almost completely devoid of NeuN staining. **(e)** same region as in (b), (c) and (d), but with only NeuN-positive staining. **(f)** same region as in (b), (c), (d) and (e) with NeuN and GFP staining merged. Notice that GFP-positive staining (b,f) is confined to the ventral midline of the thalamus, in the region of the ReRh nucleus, and that the spread of neurodegeneration (d,e,f) is well superimposed with that of the infection (f), as accounted for by the GFP-positive staining. Dimensions of the scale bar are shown directly on the photographs.

an extra band indicates the absence of any virus contamination. Furthermore, we could not exclude a priori that subsequently to the nuclear production of the fused CreGFP protein, the recognition of NeuN by the anti-NeuN antibody could have been altered (e.g., due to epitope masking). Therefore, we performed additional immunostaining with antibodies raised against either calbindin or calretinin, two calcium-binding proteins expressed by ReRh neurons either separately or conjointly, and characterizing different neuronal subpopulations of this thalamic brain region (Viena et al., 2021). This additional staining confirmed that, in the vicinity of the AAVrg-Cre-GFP

injection/transduction site, both single- and dual-labelled cells had almost completely disappeared (see supplementary Fig. 5). This observation confirmed that neurons were actually lost.

Were these observations specific to the VMT, which, for unknown reasons, might have shown a particular fragility to the viral infection or the AAV2 serotype? To address this question, we injected 2×0.5 µL of AAVrg-Cre-GFP into the medial prefrontal cortex (mPFC) of 6 rats, at a titer of 1.25×10^{13}. After a postsurgical survival time of 5 weeks, we also found evidence for neuronal degeneration in the mPFC (supplementary Fig. 6), indicating that the neurotoxicity was apparently not specific to a particular brain region. Again, DAPI staining appeared normal in the region of the mPFC that revealed devoid of neurons (not illustrated). Similar observations were made in rats injected with 3×0.6 µL of AAVrg-Cre-GFP on each cortical side after a post-surgical survival time of 10 weeks (not illustrated).

The combination of the intrathalamic injection of the AAVrg-Cre-

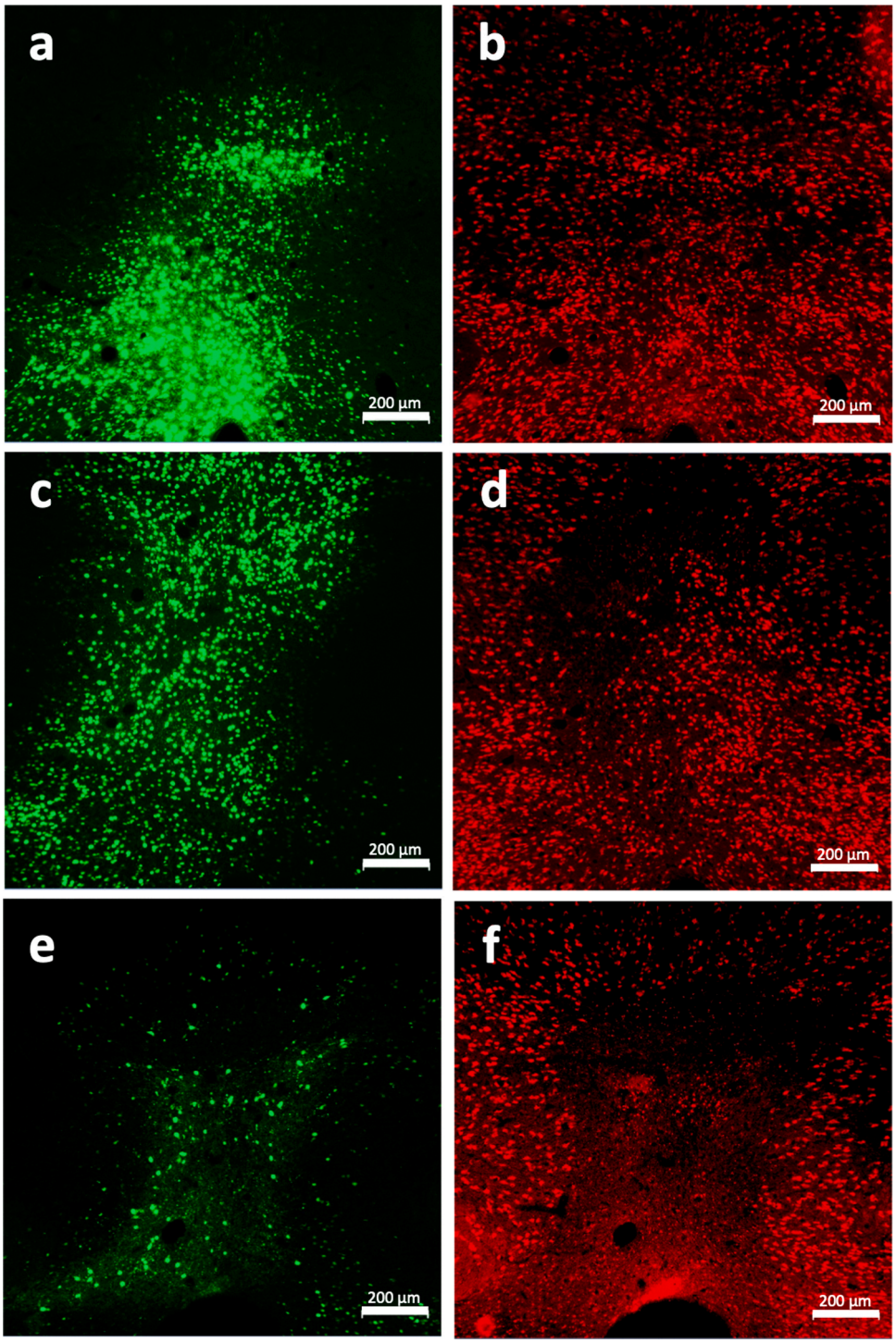

Fig. 3. Illustrations of the transduction found in the ReRh nuclei at post-injection delays of 1 **(a,b)**, 2.5 **(c,d)** and 10 weeks **(e,f)**. Rats have been injected with the AAVrg-Cre-GFP into the ReRh nuclei. **(a)**, **(c)**, **(e)** show GFP-positive nuclei in the ReRh, **(b)**, **(d)**, **(f)** show NeuN immunostaining in the same regions as shown on their left. Notice the evidence for a progressive disappearance of NeuN-positive cells within the region of transduction, which parallels a reduction of the GFP-positive signal. Dimensions of the scale bar are shown directly in the photographs.

GFP and the intracortical injection of the AAV5-taCasp constructs resulted in damage to mPFC neurons. However, information provided by DAPI and NeuN staining in the ventral midline thalamus (near-normal nuclear staining vs. neuronal depletion) appeared paradoxical, what clearly required further investigation.

3.2. Experiment 2: Time line of AAV-Cre-GFP effects

3.2.1. Neuronal toxicity

To further our investigation, based on the observations shown in Fig. 2, we decided to characterize the effects of the retrograde AAVrg-Cre-GFP at various post-injection delays, with a maximal delay of 10 weeks post-surgery. This second experiment aimed to follow the chronology of the presumed neuronal toxicity of the viral construct. Our hypothesis was that, at shorter delays, toxicity could have been weaker or even absent. Therefore, we injected 2×1 μL of the retrograde AAVrg-Cre-GFP preparation into the ReRh nuclei, using the same titration as in experiment 1 (i.e., 1.25×10^{13} vg/mL). As we only focused on the possible toxicity of AAVrg-Cre-GFP, no AAV5-taCasp construct was systematically injected into the prefrontal cortex. The rats were killed at postsurgical delays of 1, 2.5, and 10 weeks. Data are illustrated in Fig. 3. Evidence for transduction was found at all post-surgical delays, with an overall picture of fluorescence at 10 weeks post-surgery that was attenuated compared to that observed after 5 weeks in experiment 1 (Figs. 3a, 3c, 2b and 3e). At earlier time points (Figs. 3a and 3c), the amount of GFP-positive cells in the VMT was clearly larger. Because of these apparent differences, we decided to quantify the extent of the area in which fluorescence was increased in comparison with the background. We also quantified the intensity of the GFP signal (see Experimental procedures) and the density of NeuN-positive nuclei in this area (see supplementary Fig. 1). Identical quantifications were performed on the histological material obtained in Experiment 1, thus corresponding to the 5-week post-surgical delay. Whereas the extent of the area of GFP fluorescence appeared relatively constant across delays, we observed a delay-dependent decrease of the GFP signal intensity: the longer the delay, the weaker this intensity (Figs. 3a, 3c, 2b and 3e). In parallel, we observed a progressive decrease of the density of NeuN-positive nuclei in the VMT (Figs. 3b, 3d, 2e and 3f). This was confirmed by an analysis of our quantitative data (Fig. 4). Regarding the extent of the transduction area, a one-way ANOVA showed no significant Delay effect ($F_{(3,15)} = 0.23$, $p = 0.87$). A Kruskal-Wallis (K-W) one-way ANOVA of the intensity of GFP-positive clusters within the transduction limits showed a significant Delay effect ($p < 0.001$). Using the Dunn test to perform multiple comparisons, we found the difference between the 1-week and 10-week delays to be significant ($p < 0.002$); the other differences did not reach significance. Regarding the density of NeuN-positive nuclei, the one-way ANOVA showed a significant Delay effect ($p < 0.0001$). Multiple comparisons (Newman-Keuls test) showed significant differences between the 10-week and either the 1-week ($p < 0.001$) or the 2.5-week ($p < 0.001$) delays; and between the 5-week and either the 1-week ($p < 0.01$) or the 2.5-week ($p < 0.01$) delays; the difference between 5 and 10 weeks did not reach significance. The extent of the area of neuronal loss (on frontal sections; Fig. 4e) as well as the ratio between the area of neuronal loss and the area of viral transduction (Fig. 4f) were also quantified. Regarding the former, an ANOVA showed a significant Delay effect ($F(3,15) = 45.25$, $p < 0.001$). The following differences were significant: 1 week vs. 5 weeks ($p < 0.001$) and 10 weeks ($p < 0.001$); 2.5 weeks vs. 5 weeks ($p < 0.01$) and 10 weeks ($p <$

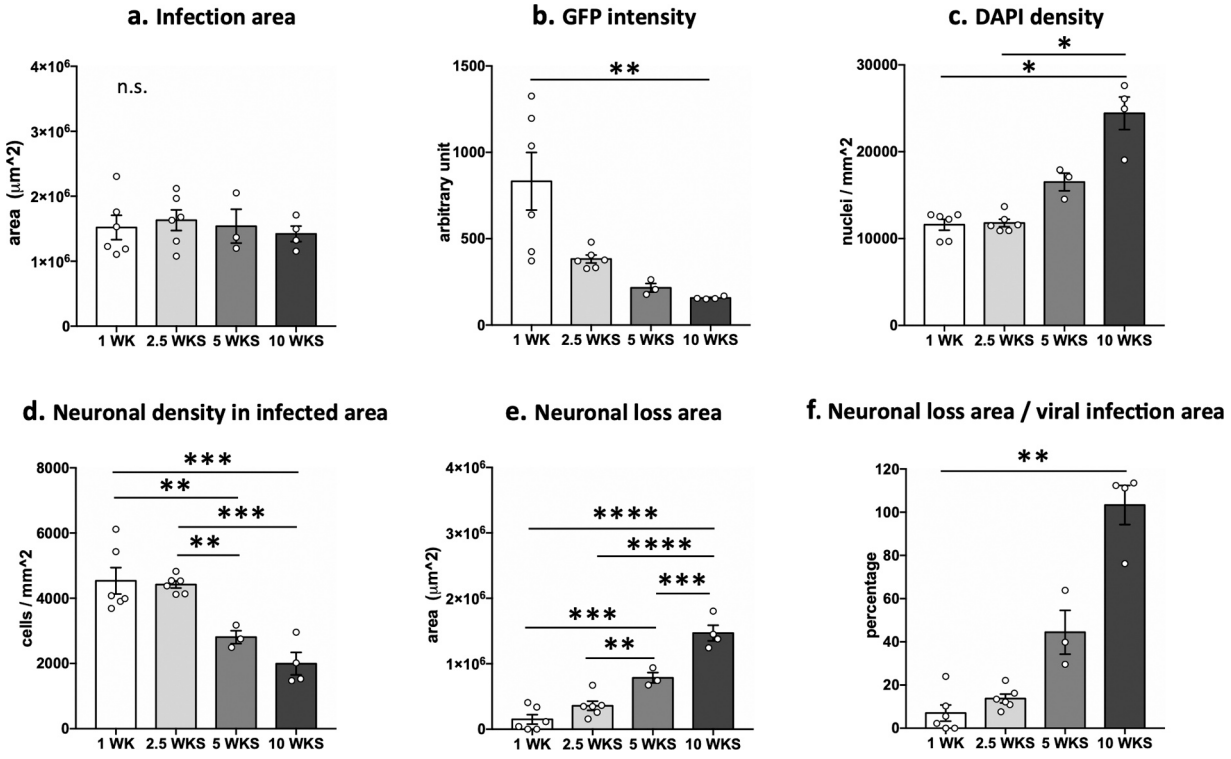

Fig. 4. Bar graphs illustrating our quantitative or semi-quantitative approaches. **(a)** Extent of the transduction area at various post-injection delays (1, 2.5, 5 and 10 weeks post-injection; data corresponding to 5 weeks are from experiment 1, the others are from experiment 2). **(b)** Semi-quantitative estimation of GFP intensity in the transduction area; the difference between 1 and 10 weeks post-injection was significant, $p < 0.01$ (**). **(c)** Quantitative estimation of DAPI density in the transduction area; at 10 weeks post-injection, the density was significantly larger than at the 1-week and 2.5-week (*, $p < 0.05$) delays; the other differences were not significant. **(d)** Quantitative estimation of the neuronal density in the transduction area; significance for the indicated differences is: **, $p < 0.01$; ***, $p < 0.001$. **(e)** Quantitative estimation of the extent of the area of neuronal loss within the region of transduction; significance for the indicated differences is: **, $p < 0.01$; ***, $p < 0.001$. **(f)** Computation of the ratio between the extent of the area of neuronal loss and the area of transduction; the difference between 1 and 10 weeks post-injection was significant, $p < 0.01$ (**).

0.001); 5 weeks vs. 10 weeks ($p < 0.001$). As to the ratio between both areas, the K-W ANOVA showed a significant Delay effect ($p < 0.001$), the only significant difference being between 1 and 10 weeks ($p < 0.01$).

Thus, taken together, these data point to an AAVrg-Cre-GFP that produced a protracted neuronal toxicity ending up, within 10 post-surgical weeks, in an almost complete loss of neurons in the region of transduction. Most of the toxic effects are reached between 2.5 and 5 weeks post-surgery. Again, as in experiment 1, DAPI staining appeared relatively constant, all along (Supplementary Fig. 7). As the DAPI density was also quantified, we performed a K-W ANOVA that showed a significant Delay effect ($p < 0.001$). With the Dunn test, we found a significant difference between the 10-week and either the 1-week ($p < 0.05$) or the 2.5-week ($p < 0.05$) delays; other differences did not reach significance.

3.2.2. Glial reactions

How can one explain that neurons undergo progressive degeneration following AAVrg-Cre-GFP injections into the VMT when the density of DAPI-stained nuclei remains apparently unchanged over the same time? Because DAPI does not distinguish between neurons and glial cells (for it stains AT regions of DNA), we hypothesized that cells within the region of transduction and neuronal loss could be glial cells reflecting a glial reaction, especially astrocytes and microglia. Indeed, astrocytes and microglia are major actors of neuroinflammation and come into play in case of neurodegeneration, whatever the latter's origin (e.g., Kwon and Koh, 2020). This is why we performed two additional immunostainings, one targeting astrocytes (with an antibody against GFAP), the other targeting microglial cells (with an antibody against Iba1). The data are illustrated in Fig. 5 and Fig. 6. At 1 week post-surgery, the GFAP immunoreactivity was virtually absent from the VMT. Clearly detectable at the 2.5-week delay, it reached a maximal staining intensity at the 5- and 10-week delays, suggesting a delay-dependent increase of astrocytic migration/reaction. A similar temporality was observed for microglial cells, the Iba1-positive staining being minimal (but not absent) at the 1-week delay and maximal at the 10-week delay. These staining signals were quantified. We measured the area covered by GFAP-positive or Iba1-positive staining, the density of cells within the stained areas, as well as the ratio between the area covered by the glial scar/region of microglial activation and that of the transduction as deduced from the GFP-positive staining. Regarding GFAP, K-W ANOVA of the area covered by the glial scar showed a significant Delay effect ($p = 0.02$). The only significant difference shown by a Dunn test was between 1 and 10 weeks ($p < 0.05$). The one-way ANOVA of GFAP density showed a significant Delay effect ($F(3,14) = 11.24$, $p < 0.001$). Multiple comparisons indicated significant differences between 1 week and either 5 ($p < 0.01$) or 10 weeks ($p < 0.001$), but also between 2.5 weeks and 5 ($p < 0.05$) or 10 weeks ($p < 0.01$). K-W ANOVA of the ratios showed a significant Delay effect ($p = 0.039$), but none of the differences reached significance. As to Iba1, one-way ANOVA of the activation area showed a significant Delay effect ($F(3,15) = 13.77$, $p < 0.001$), and multiple comparisons revealed significant differences between 1 week and 2.5 ($p < 0.05$), 5 ($p < 0.05$) and 10 weeks ($p < 0.001$), as well as 2.5 weeks ($p < 0.01$) or 5 weeks ($p < 0.05$) and 10 weeks. For the density of the Iba1 signal, a K-W ANOVA showed a significant Delay effect ($p < 0.001$), which was due to a significant difference between 1 and 10 weeks ($p < 0.01$), only. Finally, a K-W ANOVA of the ratio showed a significant Delay effect ($p < 0.001$), pairwise comparisons pointing to a larger ratio at 10 weeks as compared to 1 ($p < 0.01$) or 2.5 weeks ($p < 0.05$).

Altogether these data indicate that the AAVrg-Cre-GFP injection resulted in a progressive glial reaction, as attested for by the progressive increase of GFAP- and Iba1-positive staining. That this reaction was linked to the neurotoxic effects of the AAVrg-Cre-GFP is suggested by the high positive correlation between the area of neuronal loss and the area of microglial activation on sections passing through the ventral midline thalamus ($r = 0.924$, $p < 0.001$; see Supplementary Fig. 8).

3.3. Experiment 3: Reduction of the viral titer

Next, we tested if the injection of AAVrg-Cre-GFP using a smaller solution volume (i.e., 2×0.5 µL) and a reduced titer would result in attenuated toxicity in the ReRh nuclei. Four titers were tested: 6.25×10^{12}, 3.125×10^{12}, 1.25×10^{12}, 1.25×10^{11} vg/mL, in addition to the one used in Experiments 1 and 2. The volume/titer producing toxicity in the aforementioned experiments was not included, as we reduced the volume injected. Rats were kept for a 5-week post-surgical survival time, a delay at which we had observed strong toxicity with the highest titer used. Data are illustrated in Fig. 7. In this figure, one can see that the second lowest titer (i.e., 1.25×10^{12} vg/mL) used resulted in limited GFP-fluorescence which confined along the cannula track and showed minimal spreading in the target region. A similar picture was observed with the lowest titer (i.e., 1.25×10^{11} vg/mL; not illustrated). Clearly, the transduction was by far insufficient or even inefficient with these two titers. With the next higher titer (i.e., 3.125×10^{12} vg/mL), the transduction had spread in the ReRh nuclei and the NeuN immunostaining showed no obvious evidence for local neuronal toxicity; on some sections, however, closest to the injection site, a restricted region of limited neuronal loss could be identified. With the highest titer, the transduction appeared correct, but there was clear-cut evidence for neuronal toxicity in and around the injection site, although to a much weaker extent than with the titer used in experiments 1 and 2. All these qualitative observations were confirmed in a quantitative approach aiming at measuring the extent of the infection area, of the area showing neuronal loss, of the neuronal density therein, and of the ratio between the area of neuronal loss and that of the infection extent, as shown in Supplementary Fig. 9. It is noteworthy that even with the titer of 3.125×10^{12} vg/mL, we found quantitative evidence for limited toxicity, which was significant.

3.4. Experiment 4: Combination of the retrograde AAVrg-Cre-GFP injections into the ReRh nuclei (at a less toxic titer) with an intracortical injections of anterograde AAV5-taCasp

Next, we asked if AAVrg-Cre-GFP used at a titer of 3.125×10^{12} vg/mL in combination with an intracortical injection of the AAV5-taCasp would result in damage to cortical neurons projecting to the ReRh nuclei. To answer this question, rats were injected with both viral preparations, AAV5-taCasp in the medial prefrontal cortex (same conditions as in experiment 1) and AAVrg-Cre-GFP in the ReRh nuclei (i.e., 3.125×10^{12} vg/mL). The AAV5-taCasp was injected unilaterally and the contralateral side was used as control. Histological observations are illustrated in Fig. 8. In the mPFC, we found a reduction of the number of GFP-positive cells on the side in which the AAV5-taCasp had been injected as compared to the contralateral hemisphere (Fig. 8). On the side injected with the AAV5-taCasp, the number of GFP-positive neurons was reduced by about 40 % in average as compared to the contralateral hemisphere (Fig. 8); this reduction was comparable to the one found in Experiment 1. Statistical analyses on all sections showed that this reduction was significant ($t_{(27)} = 5.790$, $p < 0.001$).

Thus, when the titer of AAVrg-Cre-GFP injected into the ReRh was reduced from 1.25×10^{13} to 3.125×10^{12} and coupled to an intracortical injection of the AAV5-taCasp, we significantly reduced the intrathalamic toxicity of the first virus and found a capability for the combination to damage part of the mPFC neurons projecting on ventral midline thalamic targets.

4. Discussion

The start point of the current series of experiments consisted in combining an AAVrg-Cre-GFP injected into the ReRh nuclei with an AAV5-taCasp injected into the mPFC in order to selectively damage neurons that project from this cortical region to the ventral midline thalamus (VMT). While a proportion of neurons in the mPFC were

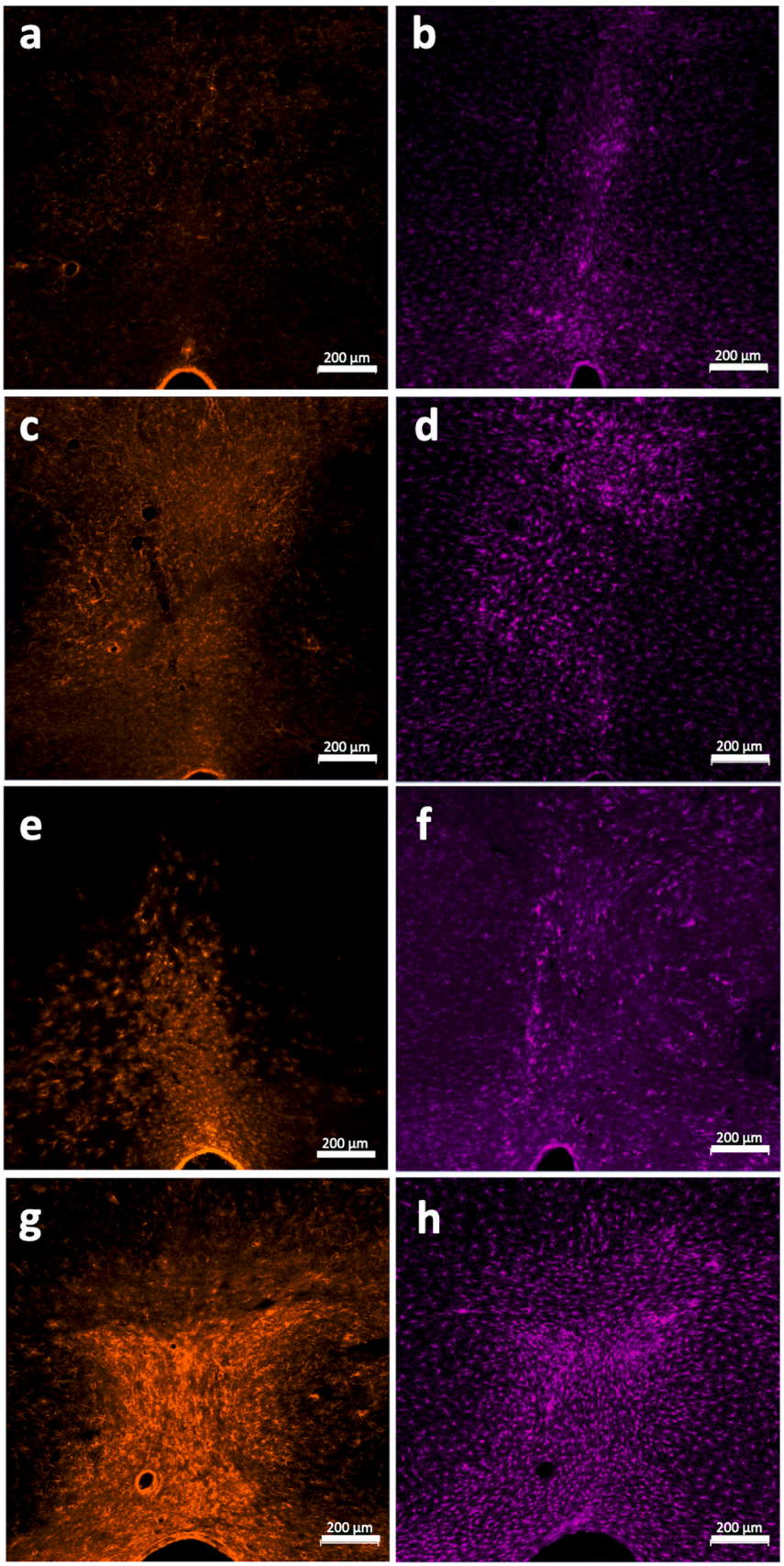

Fig. 5. Images showing GFAP (astrocytes; on the left) and Iba1 (microglia; on the right) immunostaining in the region of transduction at various delays after the injection into the ReRh nuclei of the AAV-Cre-GFP, namely 1 week **(a,b)**, 2.5 weeks **(c,d)**, 5 weeks **(e,f)**, and 10 weeks **(g,h)**. Notice the delay-dependent increase of staining accounting for reactive astrocytes and microglia. Dimensions of the scale bar are shown directly on the photographs.

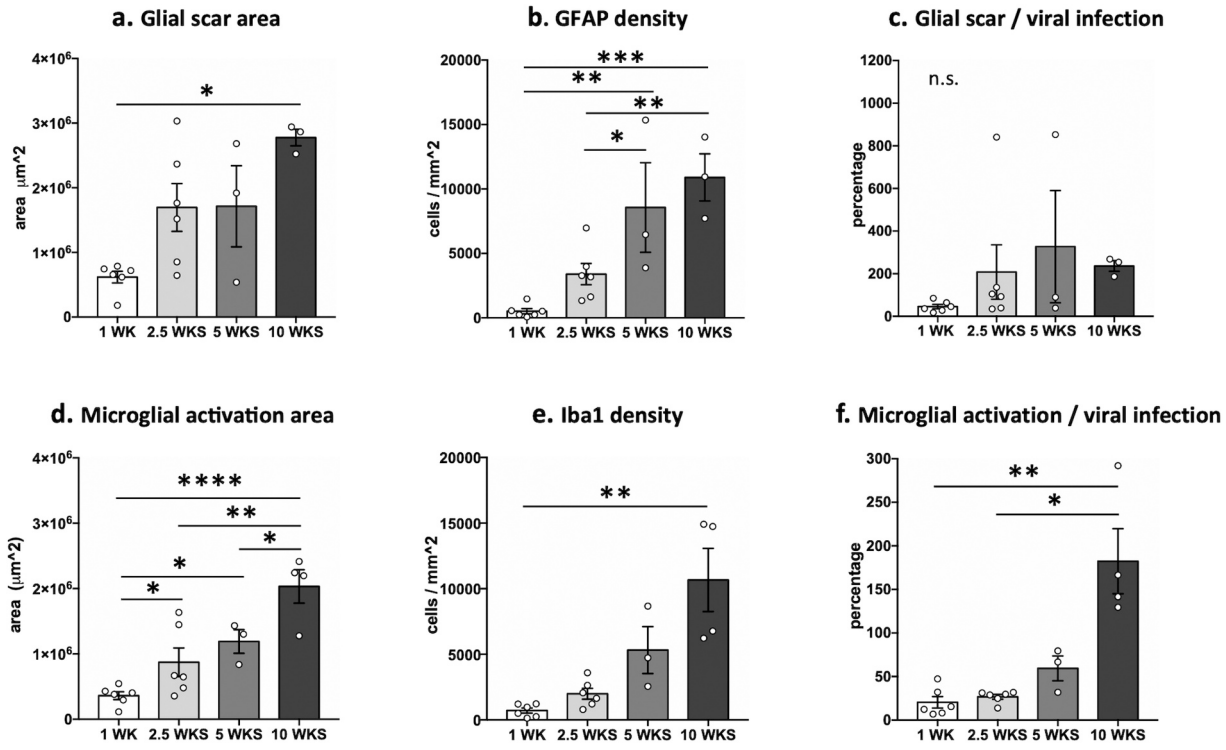

Fig. 6. Bar graphs illustrating our quantitative approaches of the histological material illustrated in Fig. 5. **(a)** Extent of the glial scar at various post-injection delays (1, 2.5, 5 and 10 weeks; data corresponding to 5 weeks are from experiment 1, the others from experiment 2); the difference between 1 and 10 weeks post-injection was significant, $p < 0.05$ (*). **(b)** Quantitative estimation of GFAP staining density in the transduction area; at 10 weeks post-injection, the density was significantly larger than at the 1-week (***, $p < 0.001$) and 2.5-week (**, $p < 0.01$) delays, and at 5 weeks post-injection, the density was also significantly larger than at 1 week (**, $p < 0.01$) and 2.5 weeks (*, $p < 0.05$). **(c)** Computation of the ratio between the extent of the area of the glial scar and the area of transduction; no difference was significant. **(d)** Quantitative estimations of the extent of the glial scar at the various post-injection delays; analyses showed a progressive extension of the zone over time; significance for the indicated differences is: *, $p < 0.05$; **, $p < 0.01$; ***, $p < 0.001$. **(e)** Quantitative estimation of the density of Iba1 staining in the transduction area over time; the difference between 1 and 10 weeks post-injection was significant, $p < 0.01$ (**). **(f)** Computation of the ratio between the extent of the area of microglial activation and the area of transduction; the difference between 1 and 10 weeks post-injection was significant, $p < 0.01$ (**), as well as that between 2.5 weeks and 10 weeks, $p < 0.05$ (*).

actually killed, we observed an unexpected and ultimately massive neurotoxicity of the AAVrg-Cre-GFP in the ReRh. Such neurotoxicity, which was also found when the viral construct was injected into the mPFC, contrasted with an apparently normal or slightly increased density of DAPI-positive nuclei. Staining of reactive astrocytes and microglial cells demonstrated a progressively increasing density of these cells within the limits of the viral transduction. By reducing the viral titer (to a 3.125×10^{12} vg/mL concentration + injecting half the volume, i.e., 2×0.5 µL, in the ReRh), we obtained a reduction of the toxicity in the ReRh, but kept the possibility to induce an at least partial but targeted disconnection between the mPFC and the ReRh nuclei.

4.1. Neuronal ablation a combination of virus-delivered Cre and Cre-dependent caspase

Cre-dependent caspase has been used to selectively ablate populations of neurons of the central nervous system in recent studies. A typical approach consists in using transgenic mice (or rats) preferentially expressing Cre in particular neurons of the brain. These regions are then infected with a viral vector carrying a floxed caspase (e.g., Basting et al., 2018; Bossert et al., 2023; Hatter and Scott, 2023; Laurent et al., 2017; Mazuski et al., 2020; Nadel et al., 2020; Walker et al., 2022; Whylings et al., 2021). In the current study, we combined the injection of two AAV vectors, one retrograde with both the Cre and a reporter genes injected into the ReRh nuclei, and another one, anterograde, with the caspase gene injected into the mPFC. Our goal was to specifically damage neurons of the mPFC that project to the ventral midline thalamus. To the best of our knowledge, it is the first time that such an approach targeting mPFC to ReRh projections is performed in rats. The combination of a Cre-containing AAV with a caspase-containing AAV has been the methodological option in at least one other study, which aimed to damage the neurons of the median preoptic nucleus projecting to the paraventricular nucleus (Marciante et al., 2020). In a previous study, Xu and Südhof (2013) had blocked the projections from the mPFC to the Re. However, they bilaterally injected a 2xFlx-TetTox AAV into the mPFC and a WGA-cre AAV into the Re and subsequently assessed contextual fear generalization, which was affected by the selective blockade. If one disregards the undesired effects of AAVrg-GFP-Cre in the ReRh nuclei, our histological verifications demonstrate the feasibility of the combined anterograde and retrograde AAV approach. Indeed, for AAVrg-GFP-Cre, whether with a viral titer causing neurotoxicity in the VMT (Fig. 1) or with a titration reduced by a factor 4 and half the volume injected (Fig. 8), we have been able to observe an about 40% reduction of the number of GFP-positive neurons on the injected side of the mPFC as compared to the contralateral control side. Obviously, this finding does not allow us to conclude that we have destroyed neurons projecting from the mPFC to the ReRh nuclei in a proportion that would be sufficient to induce detectable behavioural alterations. To do this, one would need to have AAV5-taCasp bilaterally in the mPFC and test the rats in a battery of behavioural evaluations that have proved sensitive to damage to the ReRh nuclei (e.g., the cognitive shifting test used by Cholvin et al., 2013, or the systemic memory consolidation tests used by Loureiro et al., 2012, or Quet et al., 2020). Moreover, in the current study, despite our various quantifications, it was not possible to know what proportion of cortical neurons have been destroyed among all cortical neurons projecting to the ReRh nuclei. There were at least

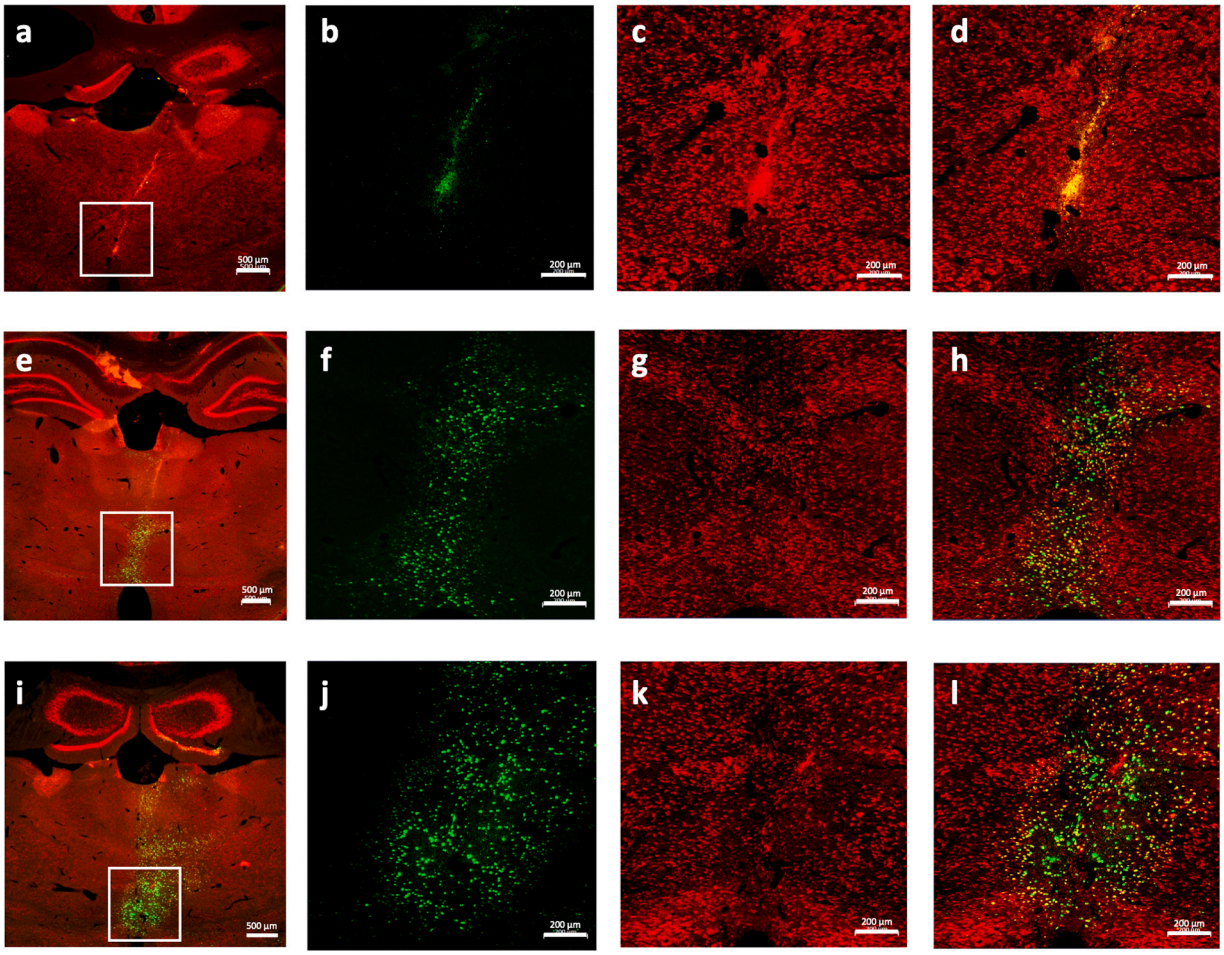

Fig. 7. Images showing the localization of the transduction in the ReRh nuclei on sections immunostained for the neuronal nuclear protein NeuN. Compared with experiments 1 and 2, the volume injected at each injection site was divided by 2 (i.e., 0.5µL instead of 1µL/site). In this experiment, we also reduced the titer. **(a-d)** are from rats injected with the AAV-Cre-GFP virus at a titer of 1.25×10^{12} vg/mL. **(e-h)** are from rats injected with the AAV-Cre-GFP virus at a titer of 3.125×10^{12} vg/mL. **(i-l)** are from rats injected with the AAV-Cre-GFP virus at a titer of 6.25×10^{12} vg/mL. The post-injection delay was of 5 weeks in all cases. On the left **(a, e, i)**, NeuN and GFP are merged and low magnification indicates the location of the transduction region. All other photographs show a higher magnification focusing on the transduction region: GFP fluorescence is shown alone in **(b,f,j)**, NeuN staining is shown alone in **(c,g,k)**, and a merge of both is shown in **(d,h,l)**. Notice that with the lowest titer the transduction was extremely limited, which is not the case with the two other titers; we found no evidence for toxicity. With the titer of 6.25×10^{12} vg/mL, we obtained a good transduction, but neuronal toxicity was observed. With the titer of 3.125×10^{12} vg/mL, the transduction was still acceptable, but we found no evidence for neurotoxicity. Dimensions of the scale bar are shown directly in the photographs.

two reasons for this: first, the number/proportion of cortical neurons projecting to the ReRh nuclei is not known; second, we have no idea about the proportion of mPFC neurons projecting to the ReRh nuclei that have been labelled with the retrograde virus.

4.2. *Neurotoxicity of the GFP-Cre fusion protein or of Cre*

Our current report is the first to show neurotoxicity of AAVrg-Cre-GFP when the viral construct is injected into the VMT of rats. Such toxicity, however, is not particular to the VMT as it was also observed in the mPFC when the same viral construct was injected in this cortical region (supplementary Fig. 6; notice that the cortical lesions appeared less extended than in the ReRh nuclei, which was probably due to the fact that we injected a smaller volume of the viral construct into the mPFC). Other studies found similar results with an AAV-Cre-GFP injected in other brain regions. For instance, Rezai Amin et al., (2019) have injected AAV2.hSyn.eGFP-Cre.WPRE.SV40 into the substantia nigra of mice that survived surgery for at least 8 weeks. They found toxicity to both dopaminergic neurons in the pars compacta and GABAergic neurons in the pars reticulata, with evidence for apoptosis and autophagy in both populations of neurons. The authors of this study have raised the possibility that it is in fact the Cre-GFP fusion protein and its nuclear accumulation that has revealed toxic. Erben et al. (2022) injected an AAV1.hSyn.HI.eGFP-Cre.WPRE.SV40 unilaterally or bilaterally into the ventral tegmental area of mice. Four weeks after the injections, the number of cells immunoreactive for tyrosine hydroxylase or the dopamine transporter (DAT) was reduced to a dramatic extent, what occurred neither with an AAV1-GFP nor with an AAV9-GFP, which were used as controls. However, when an AAV-Cre was injected, neurotoxicity was also observed, indicating again that it is most probably the Cre (rather than GFP, that can also reveal cytotoxic; e.g., Ansari et al., 2016) which is responsible for the neuronal toxicity. In a still ongoing study, we confirmed toxicity of an AAV-Cre, this time without the gene coding for GFP; Panzer et al., unpublished. Indeed, and although much of the histological verifications remain to be done, after the injection into the ReRh of the AAV-Cre, NeuN-stained material clearly exhibited neurodegeneration patterns very similar to the ones reported herein after the injection of the AAV-Cre-GFP. The fact that Cre activity can be cytotoxic *per se* is not new (e.g., Janbandhu et al., 2014; Loonstra et al., 2001). For instance, the expression of the Cre transgene in the epidermis of otherwise normal mice induces tetraploidy and apoptosis (Janbandhu et al., 2014). Along the same line, when Cre is expressed in cultured cells, it

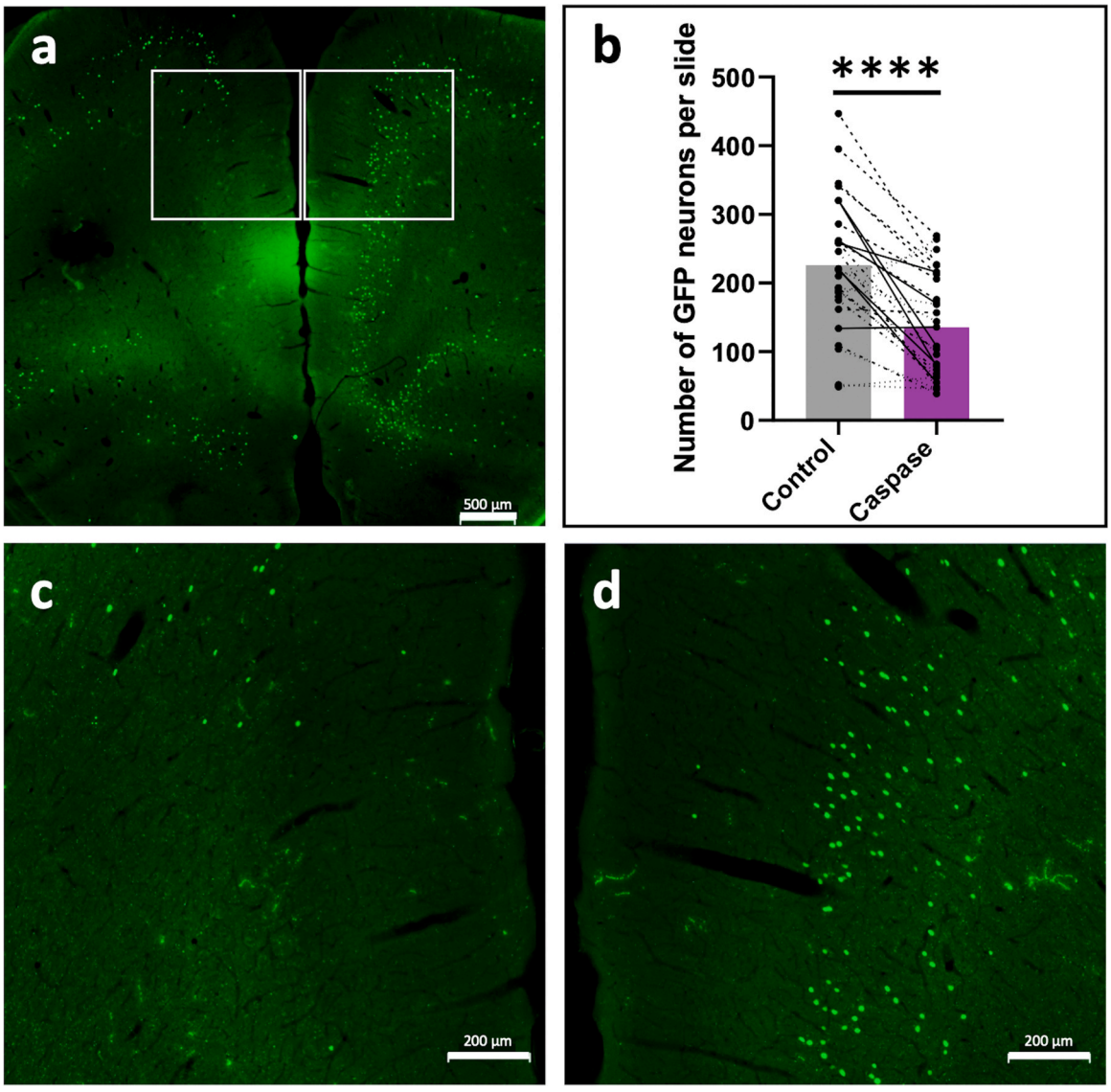

Fig. 8. The AAV containing the floxed caspase gene was injected unilaterally into the medial prefrontal cortex (mPFC) of Long-Evans male rats, which also received an injection into the reuniens and rhomboid (ReRh) nuclei of the virus containing the Cre-GFP gene coding for the fusion protein. This time, however, the titer used was the same as the one with which we found limited neurotoxicity in experiment 3 (i.e., 3.125×10^{12} vg/mL). **(a)** Image showing GFP-positive neuronal nuclei in the mPFC. **(c)** and **(d)** are higher magnifications of the cortical regions delimited by squares in (a); (c) is the side in which the AAV5-taCasp has been injected; the contralateral side (d) is used as the non-injected control. Dimensions of the scale bar are shown directly on the photographs. **(b)** Number of neurons counted on each section prepared from the brain of 3 rats (cells were counted in the mPFC ipsilateral to the AAV5-taCasp injection vs. the contralateral control side, in which no injection was made); filled circles joined by solid lines are from one rat, those joined by dashed lines are from another rat, and filled circles from the last rat are joined by stippled lines. The bars show the average value on the side injected with the AAV5-taCasp (left) and its contralateral control (right). Statistical analysis: ***, $p < 0.001$.

produces toxicity that can be related to genomic damage (Loonstra et al., 2001). When, in the current study, the viral titer was reduced, the undesirable neurotoxicity could be attenuated. This does not preclude the viral construct from being used at the titer used in our two first experiments, but specific effects would only be expected in a relatively narrow post-injection window, the duration of which remaining to be determined precisely yet. It would probably not exceed much more than a week post-injection (Fig. 4). Regarding the toxicity of the Cre protein, one could also argue that when the AAV5-taCasp is injected in the region from which the terminals infected with the AAVrg-Cre-GFP arise, neurons might not be killed by the caspase only, but also by the nuclear accumulation of Cre following retrograde infection. This possibility, which would be potentially problematic to all neurons projecting to the ReRh nuclei and obviously undermine specificity of the disconnection approach, cannot be excluded based on the results of the current study. Indeed, Cre-mediated toxicity is affecting neurons in the ReRh nuclei in the absence of caspase. Because the AAV-Cre-GFP is retroactively taken up by cortical neurons projecting to the ReRh, it also penetrates the nucleus of these projection neurons, which could be theoretically killed by the same mechanism, independently of the expression of the caspase gene. If this would be the only mechanism leading to the damage of cortical neurons projecting to the ReRh, however, one would have observed comparable damage in the mPFC in the presence as well as in the absence of the intracortical AAV5-taCasp injection. This is not what we found, as shown in Figs. 1 and 8. While a partial AAV-Cre toxicity in cortical neurons cannot be excluded, the difference between the AAV-caspase-injected side and the contralateral non-injected one clearly accounts for apoptosis-triggered toxicity on corticothalamic neurons. Furthermore, in the present study, we injected the AAV-caspase on one side only. Even if some of the cortico-thalamic neurons had been killed

by the retrograde AAV-Cre virus, we must not lose sight of the fact that this type of approach, when deployed for functional studies, is usually based on bilateral injections. In such a hypothesis, whether some of the neurons are killed by caspase and others by Cre, it seems clear that both modes of destruction would affect cortico-thalamic neurons. It cannot be ruled out, however, that Cre could kill neurons projecting to the ReRh from other structures. Current experiments (Panzer et al., unpublished), however, seem to indicate that neuronal damage by Cre in non-cortical structures projecting to the ReRh nuclei is below visual detection limits within a post-surgical time window reaching up to 12 weeks.

4.3. Glial reactions and possible confusion/misinterpretation

Degeneration of neurons is usually accompanied by an inflammatory reaction, whether in neurodegenerative diseases (Kwon and Koh, 2020; Stephenson et al., 2018) or following neurotoxic treatments, stroke, traumatic injury, infections (e.g., Hosseini and Korte, 2023; Tran et al., 2022). Inflammatory reaction implicates, among other processes, activation of astrocytes and microglia, both types of cells having also physiological functions in a healthy brain, where they are in a so-called resting state. When resting, they are for instance implicated in homeostasis regulation, blood-brain barrier maintenance, synaptic support and communication, and phagocytosis (e.g., Garland et al., 2022). Evidence for an inflammatory reaction has been obtained in the current study, as attested for by the progressive increase of reactive astrocytic and microglial signals over the weeks that followed the injection into the ReRh nuclei of the AAVrg-Cre-GFP. Indeed, after one week, there were little GFAP-positive astrocytic and Iba1-positive microglial cells in the region of viral transduction. Starting from 2.5 week after the injection, but much more so 5 and 10 weeks thereafter, the staining had increased to reach an ultimately massive level. At both later stages, almost all neurons had disappeared from the injection site. As documented by our results, the conjunction of both phenomena, namely neuronal degeneration and glial reactions, can reveal extremely misleading. Indeed, if the histological material is examined after only a DAPI staining (as done in several formerly published studies), the cellular density, as it can be deduced from the number of stained cell nuclei, appears unaltered. To achieve a precise idea of what is going on in the region in which the AAVrg-Cre-GFP was injected, it is mandatory to perform a staining accounting for the preservation of neurons. As long as this staining does not demonstrate that neurons are present in the vicinity of AAVrg-Cre-GFP injection in a near normal density, it is impossible to differentiate possible effects of the AAV5-taCasp (i.e., due to the Cre/-loxP recombination, and thus corresponding to a specific disconnection) from those of the AAVrg-Cre-GFP (i.e., due to the Cre or Cre-GFP toxicity). The picture could even be further complicated by synergistic interactions between both types of effects, thereby leading to additional confusion.

4.4. Reducing the titer, a possible solution to hamper neurotoxicity

Erben et al. (2022) have reported that neuronal toxicity of Cre-GFP could be substantially attenuated by reducing the titer of the viral preparation. Our own findings confirm that titer reduction reduces toxicity, although after a substantially weaker titer reduction (i.e., divided by 4, after half-dilution of the mother solution) than in the Erben et al. study (i.e., divided by 1000). We also found that when the highest titer was reduced by a factor 10 or 100, the transduction we obtained was largely insufficient. Regarding these results, one has to call for some degree of caution, and so for two reasons. First, we did not totally prevent toxicity but only reduced it substantially (Supplementary Fig. 9). An experiment currently running in our laboratory, however, indicates that this level of toxicity reduction in the ReRh is sufficient to preserve cognitive flexibility capacities that are blasted by an additional bilateral injection into the mPFC of the AAV5-taCasp. Second, we only assessed the effect of our titer reduction at one post-injection time point, namely 5 weeks after the infection. However, as long as the metabolic machinery of an infected neuron is functioning, there is no reason to believe that Cre-GFP synthesis is going to vanish or that nuclear metabolism might, *in fine*, be able to balance Cre-GFP production such as to keep the protein's concentration under a fatal nuclear toxicity threshold. It is well possible that by reducing the titer, rather than preventing toxicity, we have done nothing more than attenuating the slope of Cre-GFP production and thereby increasing the time window over which the neurotoxic threshold is reached. This would mean that the neurons would not, in absolute terms, be protected from toxicity, but that Cre-GFP production would take longer before becoming neurotoxic. Therefore, having observed a dramatically attenuated toxicity after 5 weeks post-injection with the reduced titer should not necessarily mean that no toxicity would be observed after an additional 5 weeks or later on. This possibility needs to be verified experimentally in a forthcoming study. In any case, the association of a retrograde AAV expressing Cre recombinase with an anterograde AAV expressing a Cre-dependent caspase should be used for experimental purposes only after having assessed that the time window in which experimental evaluations are performed, including behavioral ones, remains beyond the time at which a toxicity threshold might be reached.

The disconnection technique we have used here is of obvious interest for behavioral studies that seek to dissect the functioning of complex circuits formed by several brain structures and their interconnection systems. It should be emphasized, however, that before embarking on behavioral assessments, preliminary experiments carried out prior to these should enable the conditions for the most limited possible neurotoxicity of AAV-Cre-GFP to be defined. Indeed, should such toxicity prove unavoidable in the end, it is imperative that the experimenter has as precise an idea as possible of the post-surgical time window during which the data collected are free from any bias resulting from neurotoxicity induced by AAV-Cre-GFP.

We have used an approach combining two AAVs, one delivering a floxed gene coding for caspase and one delivering a gene coding for a Cre-GFP fusion protein. The former was injected into the mPFC, the latter into the ReRh nuclei, with the aim to damage neurons interconnecting these two brain regions. Our main finding was the severe neuronal toxicity of the AAVrg-Cre-GFP in the ReRh nuclei, although evidence was obtained that neurons of the mPFC projecting to the ReRh could actually be damaged. This toxicity was attenuated by using a reduced viral titer. The unexpected effects of the AAVrg-Cre-GFP reported herein clearly point to: **i)** the imperative need to verify the existence of potential collateral damage inherent in this type of approach because it is likely to distort the interpretation of the experimental data, and **ii)** the necessity to implement the essential controls in order to distinguish the phenotypic effects linked to this collateral damage from those linked to the desired disconnection, since, as we report here, the two types of damage can co-exist. It is also essential to know for how long neurons expressing the Cre-GFP protein remain operational after their infection.

CRediT authorship contribution statement

Pereira de Vasconcelos Anne: Writing – review & editing, Supervision, Methodology, Investigation, Formal analysis, Data curation, Conceptualization. **Stephan Aline:** Writing – review & editing, Supervision, Methodology, Investigation, Formal analysis, Data curation, Conceptualization. **Cassel Jean-Christophe:** Writing – review & editing, Writing – original draft, Supervision, Project administration, Methodology, Investigation, Funding acquisition, Formal analysis, Data curation, Conceptualization. **Panzer Elodie:** Writing – original draft, Investigation, Formal analysis, Data curation. **Grgurina Iris:** Methodology, Investigation. **Boutillier Anne-Laurence:** Methodology, Investigation. **Boch Laurine:** Writing – original draft, Investigation, Formal analysis, Data curation, Conceptualization. **Cosquer Brigitte:** Methodology, Investigation.

Declaration of Competing Interest

none.

Data Availability

Data will be made available on request.

Acknowledgements

The authors would like to wholeheartedly acknowledge Ms Marion Santisteban and Mr Olivier and Brice Bildstein, as well as Daniel Egesi and George Edomwony for their contribution to animal care. We also thank University of Strasbourg, CNRS and INSERM for their support of research, as well as the Agence Nationale de la Recherche for providing dedicated funds to the project CHARM (coord. P. Quilichini). Finally, we are grateful to Ms Charleen Dias for her help during immunostaining and the quantification of our histological material, and especially to Dr Alexis Bemelmans for very constructive discussions on toxicity of viral constructs and derived proteins.

Conflict of interest

The authors have no conflict of interest to declare.

Declaration of Generative (AI) and AI-assisted technologies in the Writing Process.

No such technologies have been used in the writing process.

Appendix A. Supporting information

Supplementary data associated with this article can be found in the online version at doi:10.1016/j.jneumeth.2024.110080.

References

Ali, M., Cholvin, T., Muller, M.-A., Cosquer, B., Kelche, C., Cassel, J.-C., Pereira De Vasconcelos, A., 2017. Environmental enrichment enhances systems-level consolidation of a spatial memory after lesions of the ventral midline thalamus. Neurobiol. Learn Mem. 141, 108–123.

Ansari, A.M., Ahmed, A.K., Matsangos, A.E., Lay, F., Born, L.J., Marti, G., Harmon, J.W., Sun, Z., 2016. Cellular GFP toxicity and immunogenicity: Potential confounders in in vivo cell tracking experiments. Stem Cell Rev. Rep. 12 (5), 553–559.

Bankhead, P., Loughrey, M.B., Fernández, J.A., Dombrowski, Y., McArt, D.G., Dunne, P. D., McQuaid, S., Gray, R.T., Murray, L.J., Coleman, H.G., James, J.A., Salto-Tellez, M., Hamilton, P.W., 2017. QuPath: Open source software for digital pathology image analysis. Sci. Rep. 7 (1), 16878 https://doi.org/10.1038/s41598-017-17204-5.

Basting, T., Xu, J., Mukerjee, S., Epling, J., Fuchs, R., Sriramula, S., Lazartigues, E., 2018. Glutamatergic neurons of the paraventricular nucleus are critical contributors to the development of neurogenic hypertension. J. Physiol. 596, 6235–6248.

Bentivoglio, M., Balercia, G., Kruger, L., 1991. The specificity of the nonspecific thalamus: the midline nuclei. Prog. Brain Res 87 53–80.

Bossert, J.M., Mejias-Aponte, C.A., Saunders, T., Altidor, L., Emery, M., Fredriksson, I., Batista, A., Claypool, S.M., et al., 2023. Effect of Selective Lesions of Nucleus Accumbens μ-Opioid Receptor-Expressing Cells on Heroin Self-Administration in Male and Female Rats: A Study with Novel *Oprm1-Cre* Knock-in Rats. J. Neurosci. 43, 1692–1713.

Cassel, J.-C., Ferraris, M., Quilichini, P., Cholvin, T., Boch, L., Stephan, A., Pereira De Vasconcelos, A., 2021. The reuniens and rhomboid nuclei of the thalamus: A crossroads for cognition-relevant information processing? Neurosci. Biobehav Rev. 126, 338–360.

Cassel, J.-C., Pereira De Vasconcelos, A., Loureiro, M., Cholvin, T., Dalrymple-Alford, J. C., Vertes, R.P., 2013. The reuniens and rhomboid nuclei: Neuroanatomy, electrophysiological characteristics and behavioral implications. Prog. Neurobiol. 111, 34–52.

Cearley, C.N., Wolfe, J.H., 2007. A Single Injection of an Adeno-Associated Virus Vector into Nuclei with Divergent Connections Results in Widespread Vector Distribution in the Brain and Global Correction of a Neurogenetic Disease. J. Neurosci. 27, 9928–9940.

Chen, Y.-H., Wu, K.-J., Hsieh, W., Harvey, B.K., Hoffer, B.J., Wang, Y., Yu, S.-J., 2021. Administration of AAV-Alpha Synuclein NAC Antibody Improves Locomotor Behavior in Rats Overexpressing Alpha Synuclein. Genes 12, 948.

Cholvin, T., Loureiro, M., Cassel, R., Cosquer, B., Geiger, K., De Sa Nogueira, D., Raingard, H., Robelin, L., Kelche, C., Pereira De Vasconcelos, A., Cassel, J.-C., 2013. The Ventral Midline Thalamus Contributes to Strategy Shifting in a Memory Task Requiring Both Prefrontal Cortical and Hippocampal Functions. J. Neurosci. 33, 8772–8783.

Dolleman-van Der Weel, M.J., Griffin, A.L., Ito, H.T., Shapiro, M.L., Witter, M.P., Vertes, R.P., Allen, T.A., 2019. The nucleus reuniens of the thalamus sits at the nexus of a hippocampus and medial prefrontal cortex circuit enabling memory and behavior. Learn Mem. 26, 191–205.

Erben, L., Welday, J.P., Murphy, R., Buonanno, A., 2022. Toxic and Phenotypic Effects of AAV_Cre Used to Transduce Mesencephalic Dopaminergic Neurons. Int J. Mol. Sci. 23, 9462.

Ferraris, M., Cassel, J.-C., Pereira De Vasconcelos, A., Stephan, A., Quilichini, P.P., 2021. The nucleus reuniens, a thalamic relay for cortico-hippocampal interaction in recent and remote memory consolidation. Neurosci. Biobehav Rev. 125, 339–354.

Garland, E.F., Hartnell, I.J., Boche, D., 2022. Microglia and Astrocyte Function and Communication: What Do We Know in Humans? Front. Neurosci. 16, 824888.

Groenewegen, H.J., Berendse, H.W., 1994. The specificity of the 'non specific' midline and intralaminar thalamic nuclei. Trends Neurosci. 17, 52–57.

Hatter, J.A., Scott, M.M., 2023. Selective ablation of VIP interneurons in the rodent prefrontal cortex results in increased impulsivity. PLoS One 18, e0286209.

Hoover, W.B., Vertes, R.P., 2012. Collateral projections from nucleus reuniens of thalamus to hippocampus and medial prefrontal cortex in the rat: a single and double retrograde fluorescent labeling study. Brain Struct. Funct. 217, 191–209.

Hoover, W.B., Vertes, R.P., 2007. Anatomical analysis of afferent projections to the medial prefrontal cortex in the rat. Brain Struct. Funct. 212, 149–179.

Hosseini, S., Korte, M., 2023. How viral infections cause neuronal dysfunction: a focus on the role of microglia and astrocytes. Biochem Soc. Trans. 51, 259–274.

Humphries, M.P., Maxwell, P., Salto-Tellez, M., 2021. QuPath: The global impact of an open source digital pathology system. Comput. Struct. Biotechnol. J. 19, 852–859. https://doi.org/10.1016/j.csbj.2021.01.022.

Janbandhu, V.C., Moik, D., Fässler, R., 2014. Cre recombinase induces DNA damage and tetraploidy in the absence of loxP sites. Cell Cycle 13 (3), 462–470. https://doi.org/10.4161/cc.27271.

Jay, T.M., Witter, M.P., 1991. Distribution of hippocampal CA1 and subicular efferents in the prefrontal cortex of the rat studied by means of anterograde transport of Phaseolus vulgaris-leucoagglutinin. J. Comp. Neurol. 313, 574–586.

Jayachandran, M., Viena, T.D., Garcia, A., Veliz, A.V., Leyva, S., Roldan, V., Vertes, R.P., Allen, T.A., 2023. Nucleus reuniens transiently synchronizes memory networks at beta frequencies. Nat. Commun. 14 (1), 4326. https://doi.org/10.1038/s41467-023-40044-z.

Klein, M.M., Cholvin, T., Cosquer, B., Salvadori, A., Le Mero, J., Kourouma, L., Boutillier, A.-L., Pereira De Vasconcelos, A., Cassel, J.-C., 2019. Ventral midline thalamus lesion prevents persistence of new (learning-triggered) hippocampal spines, delayed neocortical spinogenesis, and spatial memory durability. Brain Struct. Funct. 224, 1659–1676.

Kwon, H.S., Koh, S.-H., 2020. Neuroinflammation in neurodegenerative disorders: the roles of microglia and astrocytes. Transl. Neurodegener. 9, 42.

Laurent, V., Wong, F.L., Balleine, B.W., 2017. The Lateral Habenula and Its Input to the Rostromedial Tegmental Nucleus Mediates Outcome-Specific Conditioned Inhibition. J. Neurosci. 37, 10932–10942.

Loonstra, A., Vooijs, M., Beverloo, H.B., Allak, B.A., van Drunen, E., Kanaar, R., Berns, A., Jonkers, J., 2001. Growth inhibition and DNA damage induced by Cre recombinase in mammalian cells. Proc. Natl. Acad. Sci. USA 98 (16), 9209–9214. https://doi.org/10.1073/pnas.161269798.

Lorente de No, R., 1938. Cerebral cortex: architecture, intracortical connections, motor projections. Physiology of the Nervous System (Fulton J). Oxford University Press, London, pp. 291–340.

Loureiro, M., Cholvin, T., Lopez, J., Merienne, N., Latreche, A., Cosquer, B., Geiger, K., Kelche, C., Cassel, J.-C., Pereira De Vasconcelos, A., 2012. The Ventral Midline Thalamus (Reuniens and Rhomboid Nuclei) Contributes to the Persistence of Spatial Memory in Rats. J. Neurosci. 32, 9947–9959.

Marciante, A.B., Wang, L.A., Little, J.T., Cunningham, J.T., 2020. Caspase lesions of PVN-projecting MnPO neurons block the sustained component of CIH-induced hypertension in adult male rats. Am. J. Physiol. Heart Circ. Physiol. 318, H34–H48.

Mazuski, C., Chen, S.P., Herzog, E.D., 2020. Different Roles for VIP Neurons in the Neonatal and Adult Suprachiasmatic Nucleus. J. Biol. Rhythms 35, 465–475.

Nadel, J.A., Pawelko, S.S., Copes-Finke, D., Neidhart, M., Howard, C.D., 2020. Lesion of striatal patches disrupts habitual behaviors and increases behavioral variability. PLoS One 15, e0224715.

Paxinos, G., Watson, C., 2017. The Rat Brain in Stereotaxic Coordinates, 7th Edition. Elsevier, p. 388.

Quet, E., Majchrzak, M., Cosquer, B., Morvan, T., Wolff, M., Cassel, J.-C., Pereira De Vasconcelos, A., Stéphan, A., 2020. The reuniens and rhomboid nuclei are necessary for contextual fear memory persistence in rats. Brain Struct. Funct. 225, 955–968.

Rezai Amin, S., Gruszczynski, C., Guiard, B.P., Callebert, J., Launay, J.-M., Louis, F., Betancur, C., Vialou, V., Gautron, S., 2019. Viral vector-mediated Cre recombinase expression in substantia nigra induces lesions of the nigrostriatal pathway associated with perturbations of dopamine-related behaviors and hallmarks of programmed cell death. J. Neurochem 150, 330–340. https://doi.org/10.1111/jnc.14684.

Shen, M., Jiang, C., Liu, P., Wang, F., Ma, L., 2016. Mesolimbic leptin signaling negatively regulates cocaine-conditioned reward. Transl. Psychiatry 6 e972–e972.

Stephenson, J., Nutma, E., Van Der Valk, P., Amor, S., 2018. Inflammation in CNS neurodegenerative diseases. Immunology 154, 204–219.

Tervo, D.G.R., Hwang, B.-Y., Viswanathan, S., Gaj, T., Lavzin, M., Ritola, K.D., Lindo, S., Michael, S., et al., 2016. A Designer AAV Variant Permits Efficient Retrograde Access to Projection Neurons. Neuron 92, 372–382.

Tran, V.T.A., Lee, L.P., Cho, H., 2022. Neuroinflammation in neurodegeneration via microbial infections. Front Immunol. 13, 907804.

Varela, C., Kumar, S., Yang, J.Y., Wilson, M.A., 2014. Anatomical substrates for direct interactions between hippocampus, medial prefrontal cortex, and the thalamic nucleus reuniens. Brain Struct. Funct. 219, 911–929.

Vertes, R.P., 2004. Differential projections of the infralimbic and prelimbic cortex in the rat. Synapse 51, 32–58.

Viena, T.D., Rasch, G.E., Silva, D., Allen, T.A., 2021. Calretinin and calbindin architecture of the midline thalamus associated with prefrontal–hippocampal circuitry. Hippocampus 31, 770–789.

Walker, R.A., Suthard, R.L., Perison, T.N., Sheehan, N.M., Dwyer, C.C., Lee, J.K., Enabulele, E.K., Ray, M.H., et al., 2022. Dorsal Raphe 5-HT Neurons Utilize, But Do Not Generate, Negative Aversive Prediction Errors. eNeuro 9, ENEURO.0132-21.2022.

Weigert M., Schmidt U., Haase R., Sugawara K., Myers G. (2020) Star-convex Polyhedra for 3D Object Detection and Segmentation in Microscopy. in: 2020 IEEE Winter Conference on Applications of Computer Vision (WACV), pp 3655–3662.

Whylings, J., Rigney, N., De Vries, G.J., Petrulis, A., 2021. Reduction in vasopressin cells in the suprachiasmatic nucleus in mice increases anxiety and alters fluid intake. Horm. Behav. 133, 104997.

Xu, W., Südhof, T.C., 2013. A Neural Circuit for Memory Specificity and Generalization. Science 339, 1290–1295.

Yang, C.F., Chiang, M.C., Gray, D.C., Prabhakaran, M., Alvarado, M., Juntti, S.A., Unger, E.K., Wells, J.A., et al., 2013. Sexually dimorphic neurons in the ventromedial hypothalamus govern mating in both sexes and aggression in males. Cell 9 153 (4), 896–909.